University of Cincinnati 2016 Engine Design Competition Proposal – The Bearcat 4000

Michael Denton[1], Trace Taylor[1], Seth Young[1], Rich Zelinski[1], and Vaughn Bostwick[1]
University of Cincinnati, Cincinnati, Ohio, 45221

Abstract

Advanced materials, higher pressure ratio compressors, elevated turbine inlet temperatures, and shorter combustors have all contributed to major advances in both military and commercial engine developments. The Bearcat 4000 (BC 4000) engine is designed for the replacement of the GE-J85, currently used in the T-38 trainer aircraft. The predicted performance of the proposed afterburning turbofan engine design projects a 28% reduction in specific fuel consumption at cruise conditions compared to the J85, while still meeting thrust requirements over the flight mission. The use of a 0.35 bypass ratio resulted in a smaller core. Consequently, a 44% reduction in weight was estimated based on scaling the engine core to a modern military engine (F119), compared to the GE-J85. The three stage fan and six stage compressor designs were powered by a two stage high-pressure turbine and a two stage low-pressure turbine. A lean burning combustor with a total of nine swirl cups located radially around the annulus was designed from the constraints set by the turbomachinery designers. The use of the afterburner was only needed for supersonic dash and takeoff. Comparative studies between convergent and convergent divergent exhaust nozzle performance indicated a 8% loss in gross specific thrust at Mach 1.3 dash and a 3% loss at takeoff associated with using a convergent nozzle.

---

[1] Student, Aerospace Engineering and Engineering Mechanics, University of Cincinnati, 745 Baldwin Hall, Cincinnati, OH 45221, AIAA Student Member

I. Introduction

The Air Force has called for proposals for the replacement of the T-38 aircraft, powered with a new engine capable of exceeding the performance of the previously used GE-J85-5A afterburning turbojet engine. An emphasis on low acquisition cost and improved fuel economy has been targeted. Table 1.1 lists the chapter titles and their page number. Tables 1.2 through 1.4 provide the values required in the RFP. Appendix A includes additional cycle analysis information from Gas Turb, and Appendix B includes additional fan and compressor data.

The turbofan cycle trade-off studies were conducted based on an eleven segment mission for the trainer aircraft. Figure 1.1 shows that the Bearcat 4000 met or exceeded thrust requirements through the mission.
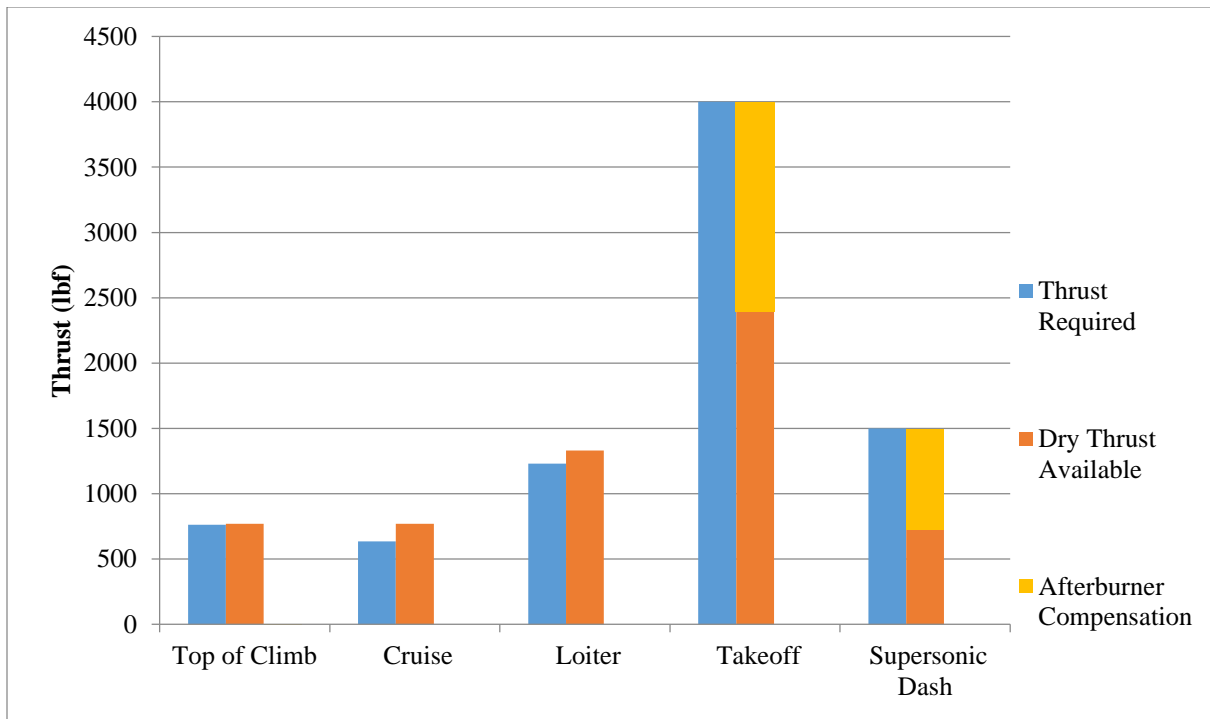

Figure 1.1. Available & Required Thrust.

Content	Page
Constraint Analysis	5
Mission Analysis	7
Cycle Analysis	10
Inlet Design	15
Turbomachinery Design	17
Combustor Design	35
Nozzle Design	46
Engine Overview	48
Summary	53
Signature Page	63

Table 1.1. Report Sections

General characteristics	
Wing area	170 ft^2
Max. take-off weight	12,000 lbm
Takeoff-Thrust	4003.01 lbf
Design Afterburning Thrust	4003.01 lbf
Performance	
Maximum speed	Mach 1.3
Cruise speed	Mach 0.85
Mission Fuel Burn	4392 lbm
Cruise TSFC	0.835 lb/lb/hr
Takeoff TSFC	1.64 lb/lb/hr
Engine Weight	218 lbm
Fan Diameter	17.6 in
Required Trade Studies	
Aircraft Constraint Diagram Page #	6
Engine Cycle Design Space Carpet Plots Page #	11
In-Depth Cycle Summary Page #	13
Final engine flowpath (Page #)	47
Detailed turbomachinery design information	
Fan	17
Compressor	17
High Pressure Turbine	25
Low Pressure Turbine	25
Detailed design of velocity triangles	
Fan	22
Compressor	23
High Pressure Turbine	31
Low Pressure Turbine	32

Table 1.2. Compliance Matrix 1

Summary Data	
Design MN	0
Design Altitude	0
Design Fan Mass Flow	43.434 lbm/s
Design Gross Thrust	4003.01 lbf
Design Bypass Ratio	0.35
Design Net Thrust	4003.01 lbf
Design Afterburning Net Thrust	4003.01 lbf
Design TSFC	1.64 lb/lb/hr
Design Overall Pressure Ratio	40.39
Design T4.1	2546.2 R
Design Fan / LPC Pressure Ratio	2.9
Design Chargeable Cooling Flow (%@25)	6%
Design Non-Chargeable Cooling Flow (%@25)	0
Design Adiabatic Efficiency for Each Turbine	
High Pressure Turbine	0.85
Low Pressure Turbine	0.89
Design Polytropic Efficiency for Each Compressor	
Fan	0.89
Compressor	0.89
Design HP/IP/LP Shaft RPM	
High Pressure Shaft	35000 RPM
Low Pressure Shaft	17000 RPM
Additional Information	
Design HP/LP Shaft Off-take Power	50 hp
Design Customer Bleed Flow	2.17 lbm/s

Table 1.3. Summary Matrix

Flow Station Data					
	Fan	Compressor	Combustor	HPT	LPT
Inflow (lbm/s)	43.434	32.17	30.24	30.66	32.59
Corrected Inflow (lbm/s)	45	13.493	1.37	1.77	10.54
Inflow Total Pressure (psia)	14.55	42.62	587.71	564.2	81.44
Inflow Total Temperature (°R)	545.67	767.21	1697.41	2546.2	1664.35
Inflow Fuel-air-Ratio	0	0	0	0.015	0.013
Inflow Mach #	0.5	0.51	0.26	0.2	0.25
Inflow Area (ft^2)	1.28	0.37	0.06	0.13	0.34
Pressure Loss/Rise Across Component	2.9	13.79	0.96	6.86	2.16

Table 1.4. Flow Station Data

II. Constraint Analysis

The objective of the constraint analysis is to find the thrust loading (T_{SL}/W_{TO}) and wing loading (W_{TO}/S) for different segments of the aircraft's flight. Thrust loading and wing loading for each segment is then plotted in a constraint diagram to find the solution space for the aircraft. The aircraft is a mass in motion with the drag acting in the opposite direction as the velocity. The weight specific excess power is determined from the rate of change of the energy height [2].

$$P_s = \left(\frac{T-(D+R)}{W}\right) * V = \frac{d}{dt}\left(h + \frac{V^2}{2g_0}\right) \qquad [2.1]$$

To find the thrust loading and wing loading values for different mission segments, the thrust lapse α, and instantaneous weight fraction β, mission segments were calculated and listed in Table 2.1. Where

$$\alpha = \frac{T}{T_{SL}} \qquad [2.2]$$

And

$$\beta = \frac{W}{W_{TO}} \qquad [2.3]$$

Thrust Lapse and Instantaneous Weight Fraction			
Segment	α	$\beta_{initial}$	β_{final}
Takeoff	1.00	1.00	0.97
Climb	0.19	0.97	0.94
Cruise	0.16	0.94	0.82
Dash	0.38	0.82	0.80
Cruise	0.09	0.80	0.69
Descend	0.00	0.69	0.69
Loiter	0.31	0.69	0.67
Descend	0.00	0.67	0.67
Land	0.00	0.67	0.65

Table 2.1. Thrust Lapse and Instantaneous Weight Fraction

Combining equations 2.1, 2.2, and 2.3 gives equation 2.4, which relates thrust loading to wing loading through the mission.

$$\frac{T_{SL}}{W_{TO}} = \frac{\beta}{\alpha}\left\{\left(\frac{D+R}{\beta W_{TO}}\right) + \frac{P_S}{V}\right\} \tag{2.4}$$

The lift and drag polar relations are calculated as follows in equations 2.5 and 2.6.

$$C_L = \frac{n\beta}{q}\left(\frac{W_{TO}}{S}\right) \tag{2.5}$$

$$C_D = K_1 C_L^2 + K_2 C_L + C_{D0} \tag{2.6}$$

The load factor is n and q is the dynamic pressure. Combining equations 2.1-2.6 results in equation [2.7].

$$\frac{T_{SL}}{W_{TO}} = \frac{\beta}{\alpha}\left\{\frac{qS}{\beta W_{TO}}\left[K_1\left(\frac{n\beta}{q}\frac{W_{TO}}{S}\right)^2 + K_2\left(\frac{n\beta}{q}\frac{W_{TO}}{S}\right) + C_{D0} + C_{DR}\right] + \frac{P_S}{V}\right\} \tag{2.7}$$

Applying the equations above, a relation of the wing and thrust loading can be made and graphically present the solution space of the aircraft. The engine cycle design point is at takeoff. The design point is chosen to have small thrust loading and high wing loading. High wing loading will reduce wing size while low thrust loading will allow reduced engine weight.
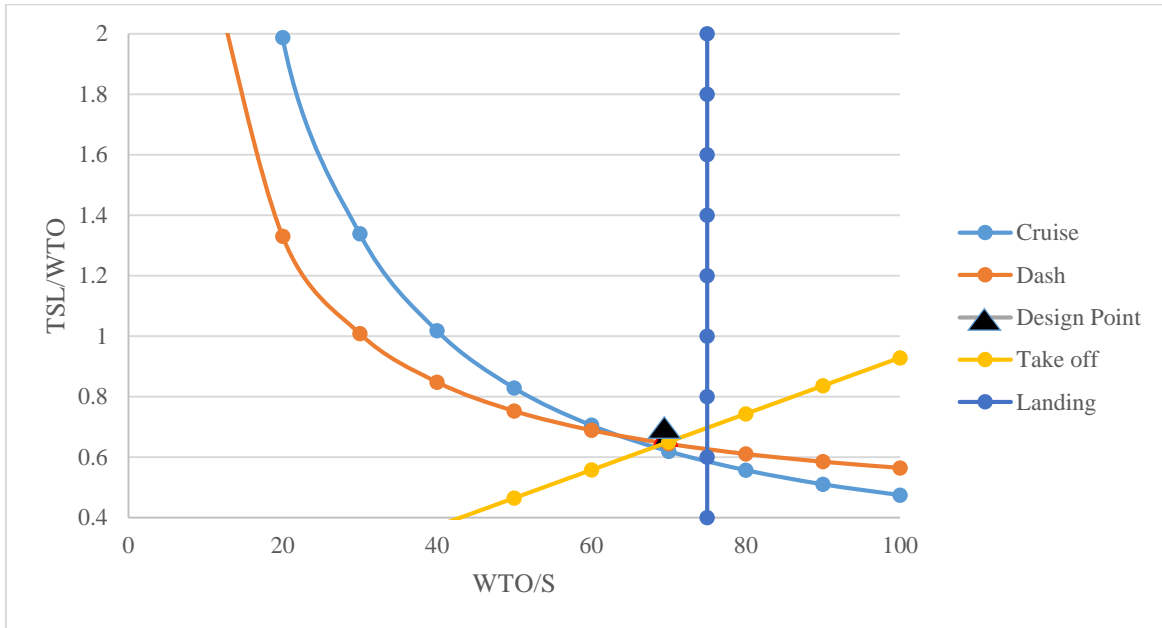

Figure 2.1. Constraint Diagram

III. Mission Analysis

Mission analysis was for a typical trainer aircraft of the T-38 class and to provide the thrust required and fuel consumption over the various mission segments. Emphasis was placed on minimizing fuel consumption and maximizing engine performance, as well as operational feasibility. Eleven segments listed in Table 3.1 were included in the mission. The table lists the calculated fuel burn during each leg of the mission as well as other performance parameters such as weight and fuel percent usage. Figure 3.1 presents the aircraft weight changes throughout the mission. An excel-based iterative mission analysis software was used to calculate amount of fuel used for each segment of the mission.

$$\frac{dW}{W} = -TSFC\frac{T}{W}dT \qquad\qquad [3.1]$$

Fuel burn was calculated using the cycle analysis in section IV to find the TSFC for each segment [Table 5.1]. The TSFC is the main variable in the equations and will determine how far and how much fuel is used for each segment.

Equation 3.1 can also be written in the form of 3.2:

$$\frac{dW}{W} = -\frac{TSFC}{V(1-u)}d(h + \frac{V^2}{2g_0}) \qquad\qquad [3.2]$$

Integrating Equation 3.2 will result in Equation 3.3:

$$\frac{W_f}{W_i} = \exp[-\frac{TSFC}{V(1-u)}\left\{(h_f - h_i) + \frac{V_f^2 - V_i^2}{2g_0}\right\}] \qquad\qquad [3.3]$$

When in steady level flight, there is no height change or speed change (i.e. Cruse), equation 3.3 changes to 3.4 [2]:

$$\frac{W_f}{W_i} = \exp[-TSFC\left\{\frac{T}{W}\right\}(t_f - t_i)] \qquad\qquad [3.4]$$

The equations presented above were used to calculate the final weight after each segment, summarized in figure 3.1.

It was shown that the most critical parts of the mission are cruise out, cruise in, and supersonic dash/military maneuvers. Cruising out to the mission uses approximately 30 percent of the fuel. Cruise back is extremely similar, but is slightly less at 25 percent because of the decreased weight of the aircraft as the mission wears on. Supersonic dash is an extremely critical mission point because although its total amount of fuel burned is low, it is the least efficient. This is because the afterburner uses a large amount of fuel, and the aircraft travels through the transonic region into supersonic cruise at Mach 1.3.
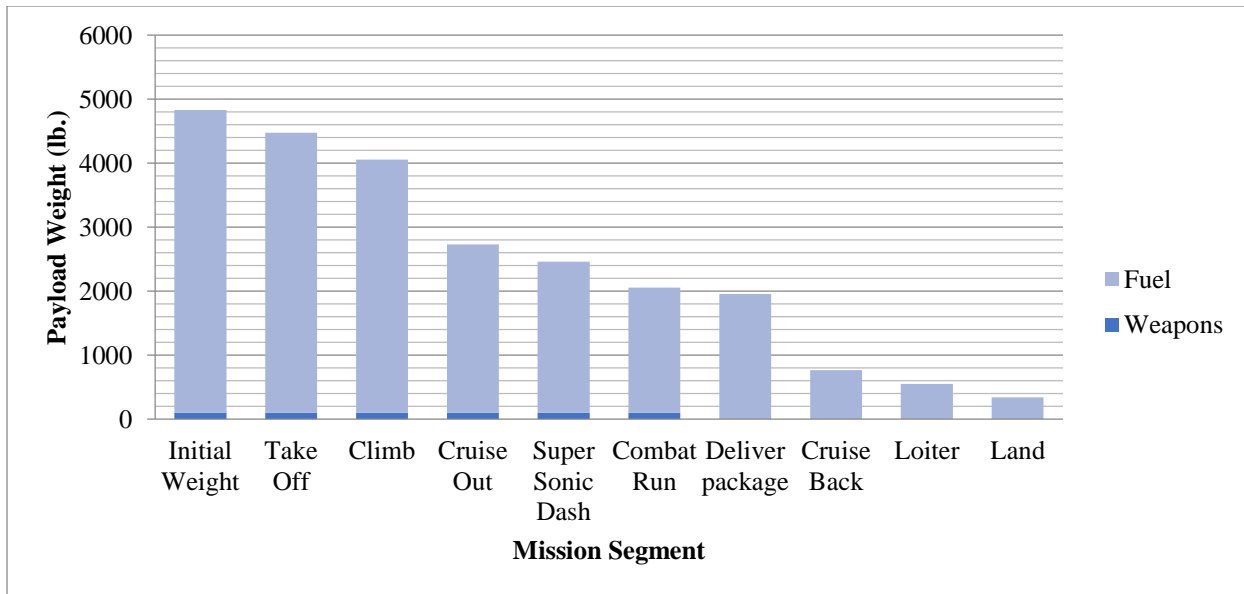

Figure 3.1. Training Mission Profile Payload Weight

Segment Number	Name	Time Estimate (min.)	Estimated Weight after segment (lbm)	Estimated Fuel Usage (lbm.)	Fuel Percent Usage	$\beta=W/W_{TO}$	W_f/W_i	Fuel left (lbm)
0	Initial		11,834			1.00		4,734
1	Takeoff	1	11,478	356	7.52 %	0.97	0.97	4,378
2	Climb to 35,00 feet	5	11,058	420	8.87 %	0.93	0.96	3,958
3	Cruise Out to M=0.8	10-15	9,733	1,325	27.99 %	0.82	0.88	2,633
4	Super Sonic Dash at M=1.3	1	9,461	272	5.75 %	0.80	0.97	2,361
5	Combat Run	10	9,058	403		0.76	0.96	1,958
6	Deliver Package	0	9,058	0		0.76	1	1,958
7	Cruise Back	10	7,865	1,193	25.20 %	0.66	0.87	765
8	Descend	5	7,840	25	0.53 %	0.66	0.997	740
9	Loiter	30	7,652	188	3.97 %	0.65	0.98	552
10	Descend	1	7,637	15	0.32 %	0.65	0.998	537
11	Land	1	7,442	195	4.12 %	0.63	0.97	342
	Total	81		4,392	92.78 %			

Table 3.1. Mission Breakdown

IV. Cycle Analysis

GasTurb was used to conduct the cycle analysis of a turbofan engine to reduce the fuel burn compared to the J85 turbojet engine. Takeoff was taken as the cycle analysis design point because it requires the maximum thrust. The request for proposal included the required thrust for each mission segment. Top of climb thrust requirement was calculated using Equation [4.1]. They are included in Table 4.1 for reference.

$$Fn_{Required} = \sin\theta \frac{TOGW}{g} + D \qquad [4.1]$$

	Takeoff (Cycle Design Point)	Cruise	Top of Climb*	Supersonic	Loiter
Thrust (lbf)	4,000	635	762.15	1,500	1,230

Table 4.1. Thrust Requirements at Each Segment (*=calculated via [4.1])

According to the RFP, the new engine is be installed in the same nacelle as the J85, which meant that the engine diameter could not exceed 20 inches. This constrained the bypass ratio to values under 0.35 to avoid turbomachinery blade heights of less than half an inch.

Trade-off studies were conducted in which the four main engine variables were varied: bypass ratio, fan pressure ratio, combustor exit temperature, and overall pressure ratio. Results are presented in Figures 4.1 through 4.5. Figure 4.1 presented the designers with the insight to chose a suitable design point. The others are further investigations on each parameter to SFC. Bypass ratios of 0.4 and above are included, however, as dotted lines in the figures. Cycle variables were chosen based on the desire to keep SFC low while keeping specific thrust high enough to meet the required thrust at each mission segment. The design point is marked by (▲) in each figure. It was chosen to minimize SFC while meeting specific thrust requirements over all mission segments.
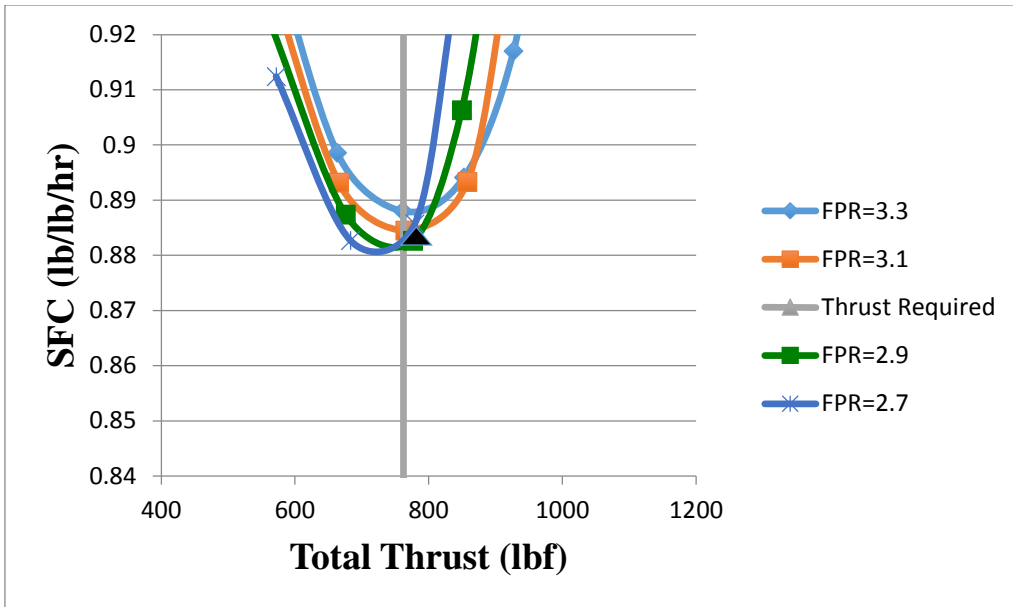
Figure 4.1. Trade-Off Optimization of FPR and T4 35kft. Altitude, Mach 0.85
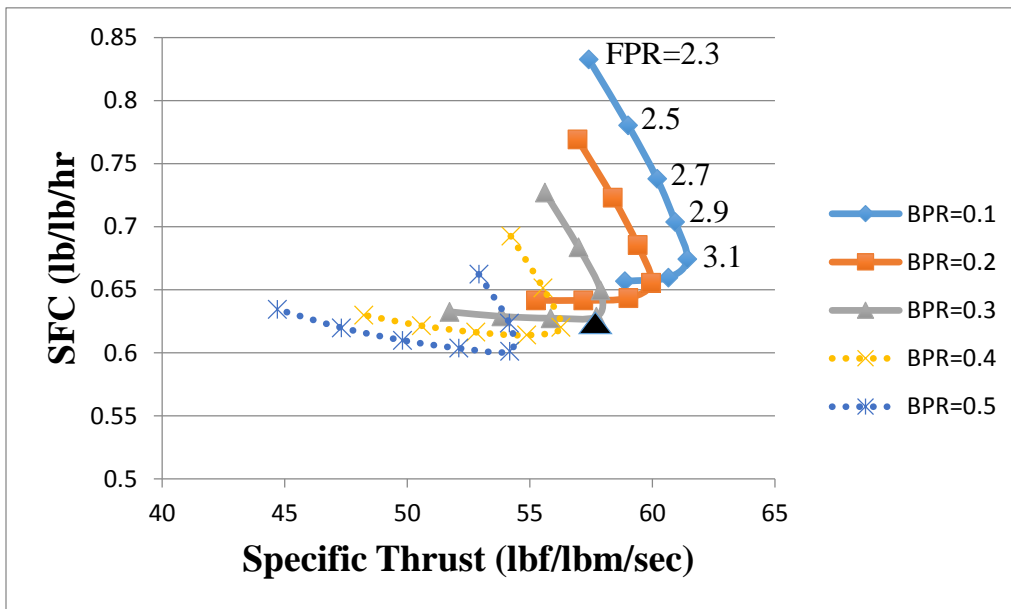
Figure 4.2. Trade-Off Optimization of BPR and FPR

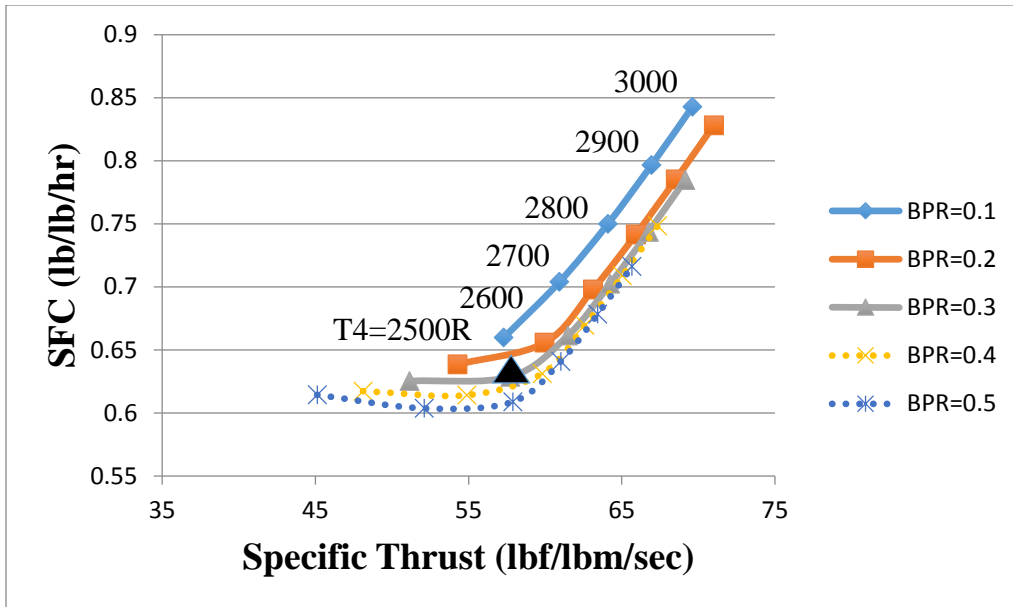**Figure 4.3**. Trade-Off Optimization of BPR and T4
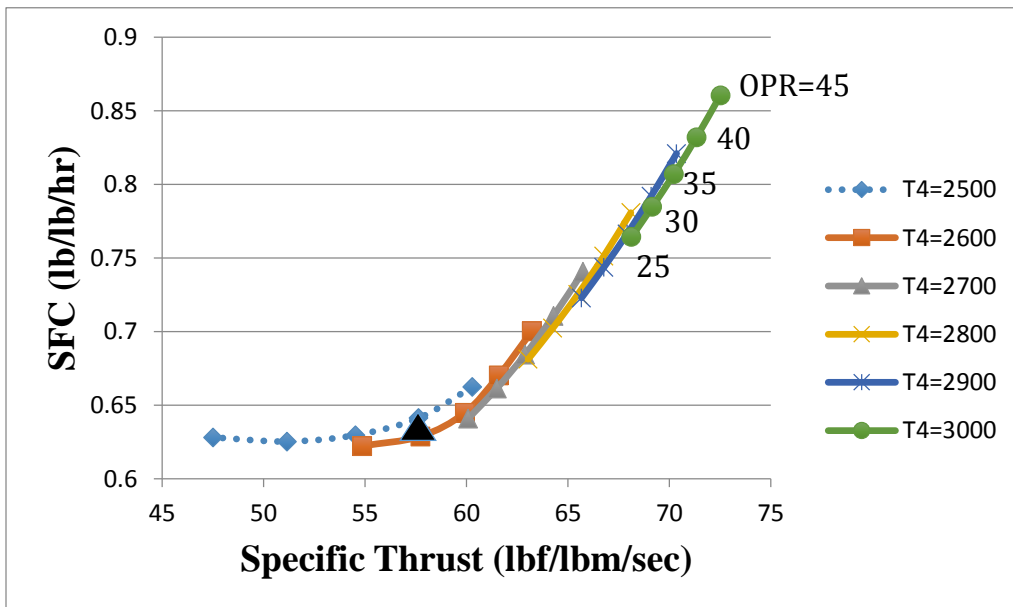
Figure 4.4. Trade-Off Optimization of T4 and OPR

Figure 4.4 represents the trade-off between combustor exit temperature and overall pressure ratio. The plot of T4 equal to 2500°R is displayed with a dotted line because it was determined that this temperature would not be sufficient to meet the required thrust at top of climb.
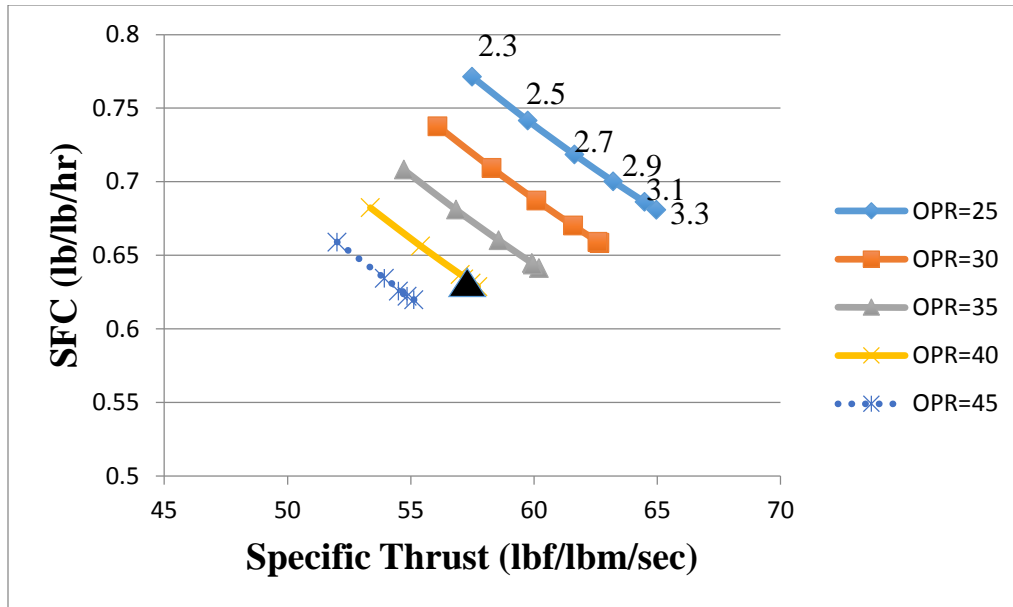
Figure 4.5. Trade-Off Optimization of OPR and FPR

Figure 4.5 represents the trade-off between overall pressure ratio and fan pressure ratio. The plot of OPR equal to 45 is displayed with a dotted line because it was determined that this pressure ratio would require compressor and turbine blades below half an inch in height, which are too small to be manufactured on the budget if a military trainer engine.

Trade-off studies yielded the final design point, displayed in Table 4.2, along with the parameters for each off-design mission segment.

	Takeoff (Design Point)	Top of Climb	Cruise	Supersonic Dash	Loiter
Total Inlet Airflow (lbm/sec)	**43.434**	18.26	17.39	21.76	29.67
Throttle (%)	**100**	100	93.6	100	96.7
Fan Pressure Ratio (FPR)	**2.9**	3.0	2.8	3	2.9
Overall Pressure Ratio (OPR)	**40.39**	46.54	40.25	39.31	39.73
Turbine Inlet Temp (T41)	**2600**	2520.3	2284.2	2565.4	2401
Bypass Ratio (BPR)	**0.35**	0.3	0.36	0.36	0.36
Afterburner Exit Temp (°R)	**3050**	NA	NA	2450	NA
Specific Fuel Consumption (lb/lb/hr)	**1.640**	0.882	0.835	1.659	0.771
Thrust (lbf.)	**4003.01**	774.02	637.05	1500.8	1234.9

Table 4.2. Cycle Analysis

Finally, results of SFC at the cruise condition of 35,000 ft. altitude and Mach 0.85 are presented for the BC 4000 turbofan engine and the J85 turbojet engine in Figure 4.6. According to this figure, the new design achieves a 28% improvement at cruise conditions over the baseline engine. This translates into a 28% improvement in range through the mission, which for the trainer aircraft application of the BC 4000, would correspond to more training hours for pilots with the same amount of fuel usage.
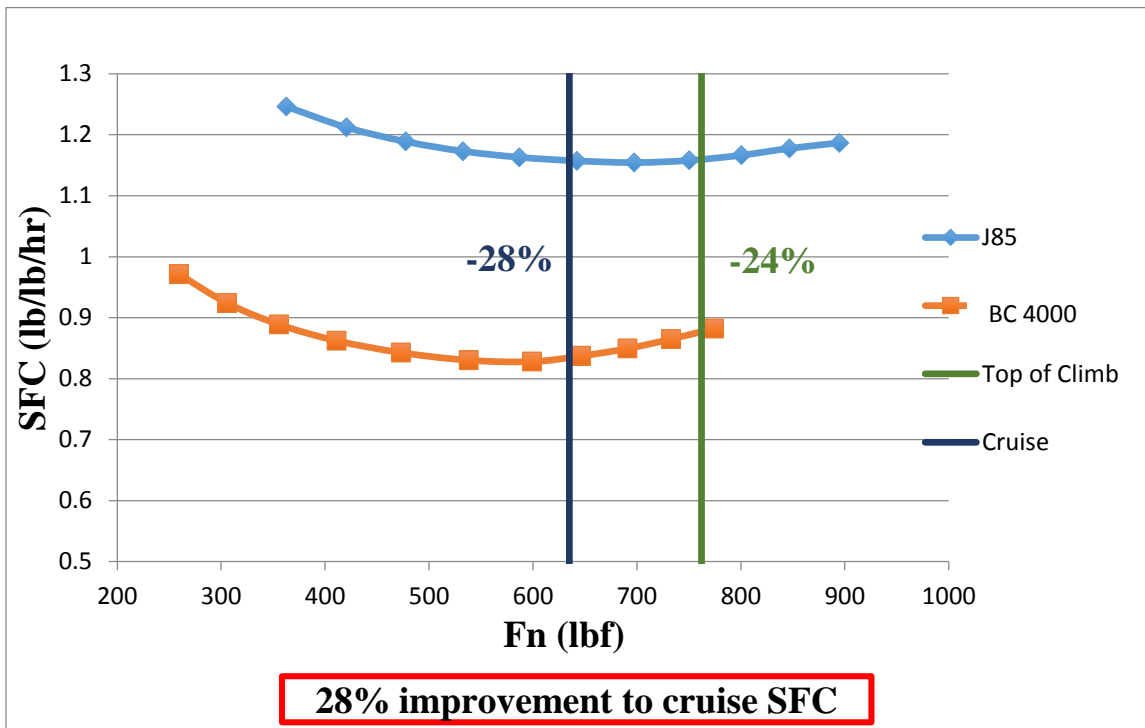
Figure 4.6. Throttle Hook Performance

V. Inlet Design

The objective of the inlet is to bring the air required for the engine from free stream conditions to the conditions needed for the entrance of the fan with minimal pressure loss and flow distortion. For this engine, both subsonic and supersonic inlet designs were considered. The difference between the two is that the subsonic inlet will operate well during low supersonic flight speed and a supersonic inlet will not perform well during subsonic conditions. To make a design choice between the two types, a comparative study was conducted by looking at the losses from the subsonic inlet going supersonically and the losses of the supersonic inlet going sub-sonically. The losses found when using a supersonic inlet while flying sub-sonically outweighed the losses of having a subsonic inlet while flying super-sonically. Due to this fact and the fact that the aircraft is subsonic throughout most of the mission, a subsonic design was chosen. Equations used to calculate the dimensions of the inlet are shown below [2].

$$D_t = \sqrt{\frac{4}{\pi} \left(\frac{m_0 \sqrt{T_{t0}}}{P_{t0}}\right)_{max} \frac{1}{MFP@M}}$$ [4.1]

Equation 4.1 can be reduced in terms of corrected mass flow

$$D_t = \sqrt{\frac{4}{\pi} \frac{\sqrt{518.7}}{2116} \frac{m_{c0\ max}}{MFP@M}}$$ [4.2]

Equation 4.2 can be further reduced to equation 4.3 which was used for the calculation of the inlet diameter D_t.

$$D_t = 0.1636\sqrt{m_{c0\ max}}$$ [4.3]

A general cross section of the subsonic inlet is shown below in Figure 4.1. Table 4.1 lists the inlet parameters.
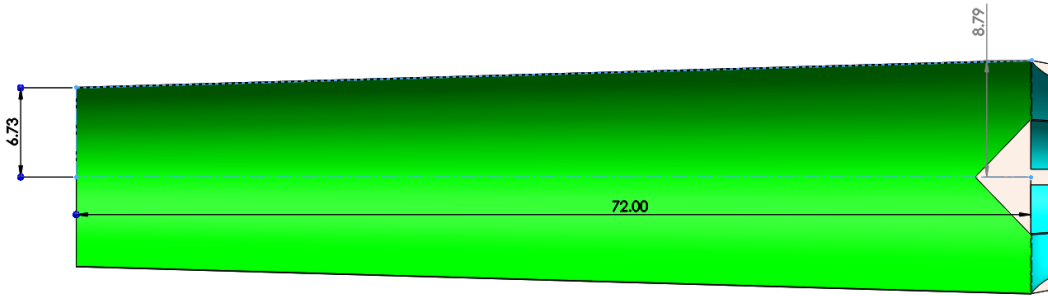
Figure 5.1. Inlet Cross Section (inches)

Face Diameter (in.)	13.47
Exit Diameter (in.)	17.6
Inlet Mach	0.85
Exit Mach	0.5
Inlet Total Pressure (psia)	5.49
Exit Total Pressure (psia)	5.43
Pressure Ratio	0.9891
Pressure Loss %	1
Length (in.)	72

Table 5.1. Inlet Attributes at Takeoff

Because it was stated in the RFP that the engine is supposed to fit into the same cell, the inlet is

unusually long. This is because the old version of the J85 has a supersonic inlet. Pressures were

calculated using the Cycle analysis from table 5.1. It is the opinion of these designers that the

aircraft designers should change or delete the existing inlet on the T-38 in order to operate an

efficient subsonic inlet. It would be recommended that the engine design team work with the

aircraft design team to adapt to an engine that will require a smaller inlet.

VI. Turbomachinery Design

A. Fan & Compressor Design

Based on the cycle trade off studies, the turbomachinery design point was selected at the top of climb where the highest corrected engine mass flow was predicted.

	Fan	Compressor
OPR	3.18	14.62
Inlet Temperature (R)	481.79	718.32
Inlet Pressure (psi)	5.5	17.48
Maximum Relative Inlet Mach Number	1.40	1.40
Axial Inlet Mach Number	0.50	0.51
Inlet Hub/Tip Ratio	0.49	0.62
De Haller Number Limit	0.70	0.74
Leiblein Diffusion Factor Limit	0.80	0.80
Pitch Line Loading Limit	0.80	1.00
Pitch Line Flow Coefficient Limit	1.00	1.00

Table 6.1 Cycle Parameters and Design Specifications at Pitch Line

For the fan and compressor constraints given by the cycle, a three stage fan and a six stage compressor were selected. The design was optimized to maintain De Haller numbers above 0.7 and Leiblein diffusion factors below 0.8 in order to minimize blade suction and surface blade separation and limit the aerodynamic losses [8].

In the preliminary design, the maximum relative Mach number was limited to 1.4 at the tip for both the transonic fan and compressor [7]. The rotational speed in the fan and compressor were constrained by the limit values on AN^2 in the LP and HP turbines to 17000 and 35000 RPM respectively.

The preliminary design was initiated and flow coefficients, and loading coefficients at the pitch line could be calculated with an axial Mach number of 0.5 at the engine face. By iterating on radii and axial Mach numbers to minimize diffusion losses, an acceptable pitch line design was completed.

	Fan			Compressor					
Stage	1	2	3	1	2	3	4	5	6
PR	1.52	1.48	1.41	1.71	1.62	1.56	1.52	1.50	1.48
Pitch Line Radii (inch)	6.57	5.80	5.22	4.24	4.25	4.15	3.99	3.81	3.54
Tip Speed (ft/s)	1306	1098	964	1604	1466	1390	1313	1237	1145
Loading Coefficient	0.56	0.69	0.63	0.99	0.73	0.60	0.48	0.43	0.31
Flow Coefficient	0.77	0.93	0.86	0.90	0.87	0.85	0.81	0.71	0.54
Reaction	0.72	0.65	0.69	0.49	0.63	0.70	0.76	0.79	0.85
Relative Mach	1.08	0.98	0.89	1.17	1.19	1.05	0.94	0.84	0.74
Axial Mach	0.50	0.60	0.61	0.51	0.80	0.69	0.61	0.53	0.43
Rotor Inlet Flow Angle	17.00	11.18	8.56	-5.00	19.86	26.20	21.56	7.43	3.46
Rotor Exit Flow Angle	47.18	46.56	41.48	49.86	53.20	54.56	47.43	35.46	29.41
Stator Exit Flow Angle	11.18	8.56	0.00	19.86	26.20	21.56	7.43	3.46	0.00

Table 6.2. Vector Diagram Summary at Pitch Line

The flow path for both fan and compressor are presented in Figure 6.1. From this point it was necessary to determine the number of blades in each stage of the fan and the compressor. Based on transonic compressor research the blade aspect ratios were chosen to be low [6]. Stagger was found using the flow angles, neglecting deviation and incidence, and blade chord lengths were then calculated. Finally, the solidity value for each blade row was assumed to be equal to the flows transonic Mach number at the inlet in each stage [7].

	Fan			Compressor					
Mean Radii (inch)	6.57	5.80	5.22	4.24	4.25	4.15	3.99	3.81	3.54
Hub/Tip Ratio	0.49	0.57	0.61	0.62	0.77	0.82	0.86	0.88	0.89
Axial Chord (inch)	2.23	1.60	1.28	1.55	0.84	0.62	0.56	0.53	0.52
Stagger Angle (°)	36.66	26.73	27.50	32.77	15.70	14.73	24.99	38.71	48.74
Blade Chord (inch)	2.77	1.80	1.44	1.84	0.87	0.64	0.61	0.69	0.79
Aspect Ratio	2.00	2.00	2.00	1.30	1.30	1.30	1.10	0.90	0.80
Solidity	1.38	1.16	1.02	1.39	1.28	1.11	1.00	1.00	1.00
Pitch	2.01	1.54	1.42	1.32	0.68	0.58	0.61	0.69	0.79
Blade Count	21	24	23	20	39	45	40	35	28

Table 6.3 Rotor Blading Parameters (Pitch Line Average)

	Fan			Compressor					
Mean Radii (inch)	5.92	5.35	4.97	4.22	4.18	4.07	3.91	3.66	3.43
Hub/Tip Ratio	0.57	0.61	0.64	0.76	0.82	0.85	0.88	0.90	0.90
Axial Chord (inch)	1.60	1.30	1.08	0.89	0.65	0.59	0.54	0.53	0.52
Stagger Angle (°)	29.18	27.56	20.74	34.86	39.70	38.06	27.43	19.46	14.71
Blade Chord (inch)	1.84	1.46	1.15	1.68	1.60	1.32	0.77	0.63	0.57
Aspect Ratio	2.00	2.00	2.00	1.30	1.30	1.10	0.90	0.71	0.67
Solidity	1.21	1.05	0.93	1.24	1.15	1.09	1.06	1.03	1.13
Pitch	1.52	1.39	1.24	1.36	1.40	1.21	0.73	0.61	0.50
Blade Count	25	24	25	20	19	21	34	37	43

Table 6.4 Stator Blading Parameters (Pitch Line Average)

With the axial Mach numbers and the pitch radii determined during the preliminary pitch line design, a flow path for the fan and compressor was drawn up.
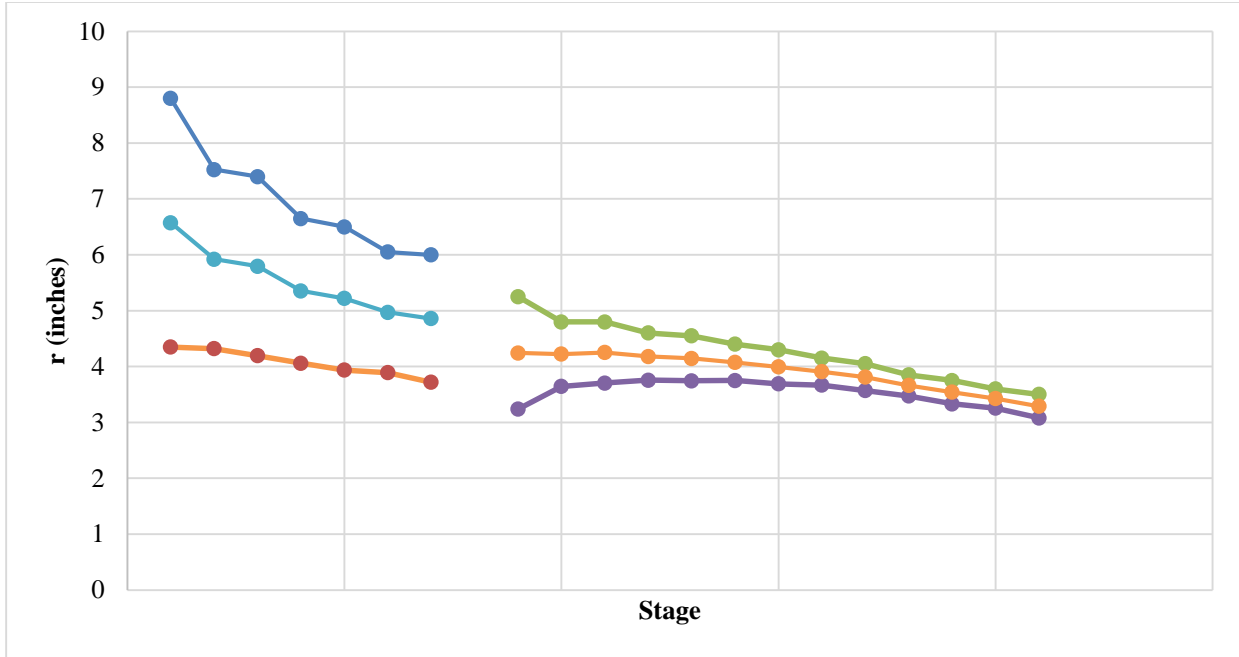
Figure 6.5 Flow Path for Fan and Compressor

The radial variation in the fan and compressor blading was based on a free vortex radial equilibrium.
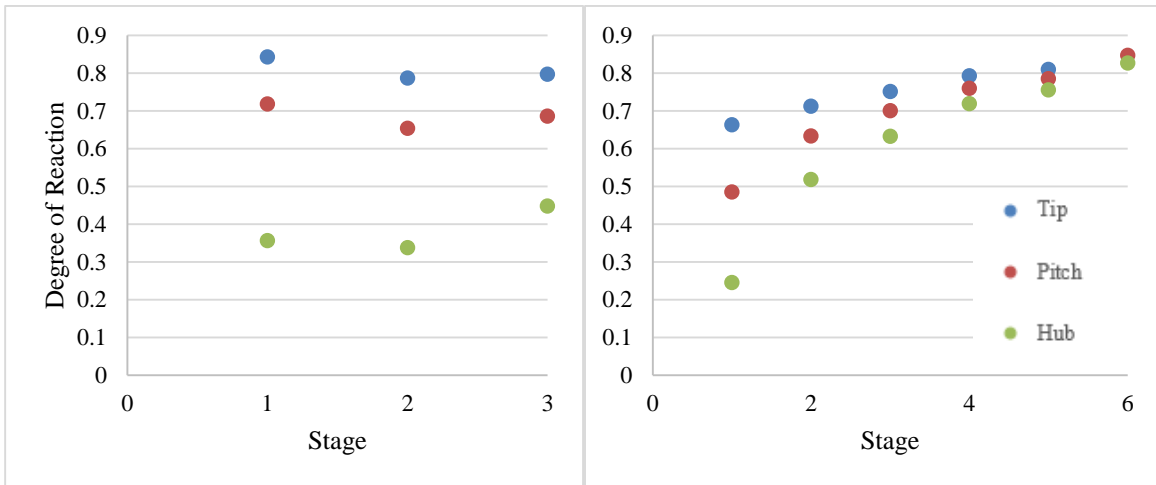
Figure 6.6a & 6.6b Degrees of Reaction for a.) Fan & b.) Compressor
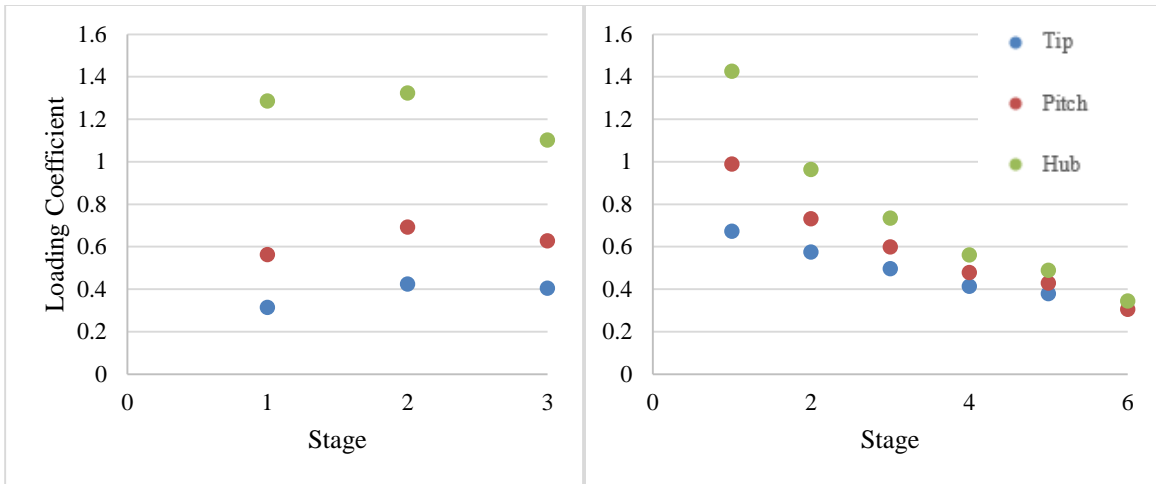
Figure 6.7a & 6.7b Loading Coefficients for a.) Fan & b.) Compressor

Figure 6.8a & 6.8b Flow Coefficients for a.) Fan & b.) Compressor

With this information, velocity triangles in Figure 6.9 were generated at the hub, pitch, and tip locations. Any values that weren't already numerically determined were calculated with basic trigonometry.

Stage 1 Tip

Beta1 = 59.875 degrees   Alpha1 = 40.5 degrees
V1 = 1009.2 ft/s   C1 = 666.11 ft/s
Cx1 = 506.51 ft/s
Vtheta1 = 872.9 ft/s   Ctheta1 = 432.6 ft/s
U1 = 1305.5 ft/s

Beta2 = 22.773 degrees   Alpha2 = 52.564 degrees
V2 = 707.21 ft/s   C2 = 1065.5 ft/s
Cx2 = 652.08 ft/s
Vtheta2 = 273.75 ft/s   Ctheta2 = 842.61 ft/s
U2 = 1116.4 ft/s

Stage 2 Tip

Alpha1 = 27.564 degrees
Beta1 = 48.68 degrees
V1 = 1001.9 ft/s   C1 = 746.25 ft/s
Cx1 = 661.54 ft/s
Vtheta1 = 752.49 ft/s   Ctheta1 = 345.32 ft/s
U1 = 1097.8 ft/s

Beta2 = 14.268 degrees   Alpha2 = 49.735 degrees
V2 = 709.42 ft/s   C2 = 1063.8 ft/s
Cx2 = 687.54 ft/s
Vtheta2 = 174.84 ft/s   Ctheta2 = 811.72 ft/s
U2 = 986.55 ft/s

Stage 3 Tip

Alpha1 = 15.935 degrees
Beta1 = 46.691 degrees
V1 = 1044.2 ft/s   C1 = 744.85 ft/s
Cx1 = 716.23 ft/s
Vtheta1 = 759.8 ft/s   Ctheta1 = 204.49 ft/s
U1 = 964.29 ft/s

Beta2 = 24.276 degrees   Alpha2 = 41.522 degrees
V2 = 736.74 ft/s   C2 = 897.01 ft/s
Cx2 = 671.59 ft/s
Vtheta2 = 302.9 ft/s   Ctheta2 = 594.63 ft/s
U2 = 897.54 ft/s

Stage 1 Pitch

Alpha1 = 17 degrees
Beta1 = 58.31 degrees
V1 = 964.19 ft/s   C1 = 529.66 ft/s
Cx1 = 506.51 ft/s
Vtheta1 = 820.43 ft/s   Ctheta1 = 154.86 ft/s
U1 = 975.29 ft/s

Beta2 = 15.017 degrees   Alpha2 = 47.18 degrees
V2 = 675.14 ft/s   C2 = 359.36 ft/s
Cx2 = 652.08 ft/s
Vtheta2 = 174.93 ft/s   Ctheta2 = 703.68 ft/s
U2 = 878.61 ft/s

Stage 2 Pitch

Alpha1 = 11.18 degrees
Beta1 = 47.784 degrees
V1 = 984.55 ft/s   C1 = 674.34 ft/s
Cx1 = 661.54 ft/s
Vtheta1 = 729.18 ft/s   Ctheta1 = 130.74 ft/s
U1 = 859.92 ft/s

Beta2 = 5.6664 degrees   Alpha2 = 46.565 degrees
V2 = 690.91 ft/s   C2 = 1000 ft/s
Cx2 = 687.54 ft/s
Vtheta2 = 68.218 ft/s   Ctheta2 = 726.16 ft/s
U2 = 794.33 ft/s

Stage 3 Pitch

Alpha1 = 8.5648 degrees
Beta1 = 42.932 degrees
V1 = 978.25 ft/s   C1 = 724.31 ft/s
Cx1 = 716.23 ft/s
Vtheta1 = 666.32 ft/s   Ctheta1 = 107.87 ft/s
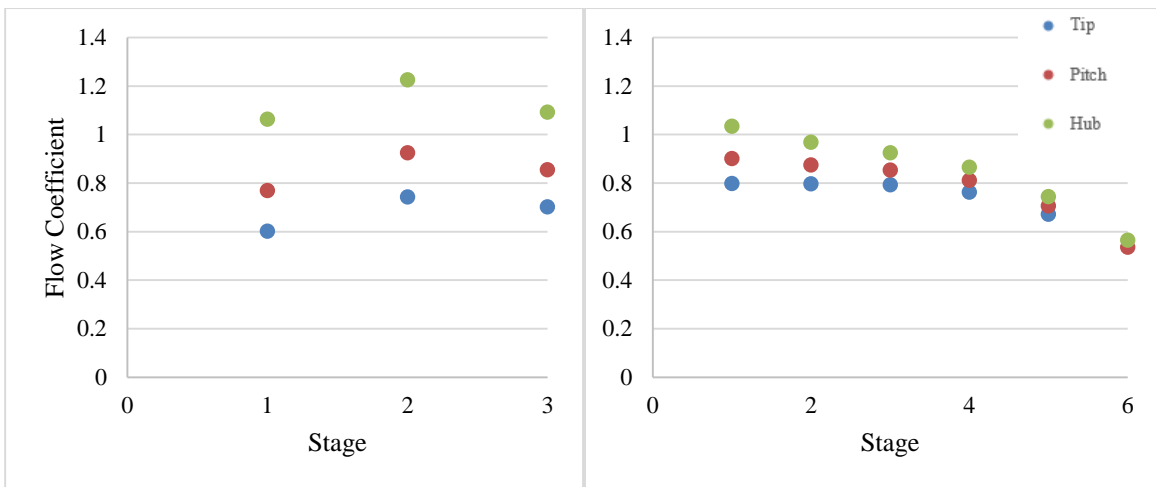U1 = 774.19 ft/s

Beta2 = 12.062 degrees   Alpha2 = 41.483 degrees
V2 = 686.75 ft/s   C2 = 896.46 ft/s
Cx2 = 671.59 ft/s
Vtheta2 = 143.51 ft/s   Ctheta2 = 593.81 ft/s
U2 = 737.33 ft/s

Stage 1 Hub

Alpha1 = 15 degrees
Beta1 = 57.028 degrees
V1 = 930.7 ft/s   C1 = 524.88 ft/s
Cx1 = 506.51 ft/s
Vtheta1 = 780.8 ft/s   Ctheta1 = 135.7 ft/s
U1 = 645.08 ft/s

Beta2 = 4.662 degrees   Alpha2 = 46.786 degrees
C2 = 952.32 ft/s
V2 = 654.25 ft/s
Cx2 = 652.08 ft/s
Vtheta2 = 53.17 ft/s   Ctheta2 = 694.04 ft/s
U2 = 640.87 ft/s

Stage 2 Hub

Alpha1 = 9.214 degrees
Beta1 = 47.791 degrees
V1 = 984.68 ft/s   C1 = 670.19 ft/s
Cx1 = 661.54 ft/s
Vtheta1 = 729.35 ft/s   Ctheta1 = 107.3 ft/s
U1 = 622.03 ft/s

Beta2 = 9.382 degrees   Alpha2 = 46.154 degrees
C2 = 992.51 ft/s
V2 = 696.86 ft/s
Cx2 = 687.54 ft/s
Vtheta2 = 113.6 ft/s   Ctheta2 = 715.8 ft/s
U2 = 602.2 ft/s

Stage 3 Hub

Alpha1 = 3.846 degrees
Beta1 = 44.435 degrees
V1 = 955.35 ft/s   C1 = 717.85 ft/s
Cx1 = 716.23 ft/s
Vtheta1 = 632.23 ft/s   Ctheta1 = 48.15 ft/s
U1 = 84.08 ft/s

Beta2 = 1.607 degrees   Alpha2 = 41.585 degrees
C2 = 897.88 ft/s
V2 = 671.85 ft/s
Cx2 = 671.59 ft/s
Vtheta2 = 18.84 ft/s   Ctheta2 = 595.96 ft/s
U2 = 577.12 ft/s

Figure 6.9. Fan Velocity Diagrams at Hub, Pitch, and Tip

22

Stage 1 Tip

- Alpha1 = 15 degrees
- Beta1 = 66.262 degrees
- W1 = 1567.1 ft/s
- C1 = 653.1 ft/s
- Cx1 = 653.1 ft/s
- Wtheta1 = 1434.5 ft/s
- Ctheta1 = 169.3 ft/s
- U1 = 1603.5 ft/s
- Beta2 = 11.462 degrees
- Alpha2 = 49.155 degrees
- W2 = 1100.4 ft/s
- C2 = 1648.9 ft/s
- Cx2 = 1078.4 ft/s
- Wtheta2 = 218.67 ft/s
- Ctheta2 = 1247.4 ft/s
- U2 = 1466.1 ft/s

Stage 2 Tip

- Alpha1 = 27.155 degrees
- Beta1 = 36.472 degrees
- W1 = 1456 ft/s
- C1 = 1315.9 ft/s
- Cx1 = 1170.9 ft/s
- Wtheta1 = 865.49 ft/s
- Ctheta1 = 600..59 ft/s
- U1 = 1466.1 ft/s
- Beta2 = 2.1031 degrees
- Alpha2 = 54.538 degrees
- W2 = 1028.3 ft/s
- C2 = 1771.3 ft/s
- Cx2 = 1027.6 ft/s
- Wtheta2 = 37.736 ft/s
- Ctheta2 = 1027.6 ft/s
- U2 = 1405 ft/s

Stage 3 Tip

- Beta1 = 32.637 degrees
- Alpha1 = 31.538 degrees
- W1 = 1315.9 ft/s
- C1 = 1300.1 ft/s
- Cx1 = 1108.1 ft/s
- Wtheta1 = 709.65 ft/s
- Ctheta1 = 680.06 ft/s
- U1 = 1389.7 ft/s
- Beta2 = 1.669 degrees
- Alpha2 = 55.917 degrees
- W2 = 927.99 ft/s
- C2 = 1655.3 ft/s
- Cx2 = 927.59 ft/s
- Wtheta2 = 27.028 ft/s
- Ctheta2 = 1370.9 ft/s
- U2 = 1343.9 ft/s

Stage 4 Tip

- Beta1 = 37.75 degrees
- Alpha1 = 25.917 degrees
- W1 = 1318 ft/s
- C1 = 1158.7 ft/s
- Cx1 = 1042.2 ft/s
- Wtheta1 = 806.93 ft/s
- Ctheta1 = 506.43 ft/s
- U1 = 1313.4 ft/s
- Beta2 = 13.401 degrees
- Alpha2 = 48.915 degrees
- W2 = 940.69 ft/s
- C2 = 1392.4 ft/s
- Cx2 = 915.08 ft/s
- Wtheta2 = 218.02 ft/s
- Ctheta2 = 1049.5 ft/s
- U2 = 1267.5 ft/s

Stage 5 Tip

- Alpha1 = 14.915 degrees
- Beta1 = 46.24 degrees
- W1 = 1364.6 ft/s
- C1 = 976.74 ft/s
- Cx1 = 943.83 ft/s
- Wtheta1 = 985.61 ft/s
- Ctheta1 = 251.4 ft/s
- U1 = 1237 ft/s
- Beta2 = 27.551 degrees
- Alpha2 = 39.533 degrees
- W2 = 984.64 ft/s
- C2 = 1131.9 ft/s
- Cx2 = 872.98 ft/s
- Wtheta2 = 455.43 ft/s
- Ctheta2 = 720.48 ft/s
- U2 = 1175.9 ft/s

Stage 6 Tip

- Alpha1 = 9.5333 degrees
- Beta1 = 52.036 degrees
- W1 = 1284.5 ft/s
- C1 = 801.22 ft/s
- Cx1 = 790.16 ft/s
- Wtheta1 = 1012.7 ft/s
- Ctheta1 = 132.7 ft/s
- U1 = 1145.4 ft/s
- Beta2 = 45.266 degrees
- Alpha2 = 32.142 degrees
- W2 = 953.98 ft/s
- C2 = 792.97 ft/s
- Cx2 = 671.43 ft/s
- Wtheta2 = 677.69 ft/s
- Ctheta2 = 421.87 ft/s
- U2 = 1099.6 ft/s

Stage 1 Pitch

- Alpha1 = 5 degrees
- Beta1 = 64.974 degrees
- V1 = 1491.2 ft/s
- C1 = 633.25 ft/s
- Cx1 = 630.84 ft/s
- Vtheta1 = 1351.2 ft/s
- Ctheta1 = 55.192 ft/s
- U1 = 1296 ft/s
- Beta2 = .5567 degrees
- Alpha2 = 49.863 degrees
- V2 = 1078.5 ft/s
- C2 = 1673 ft/s
- Cx2 = 1078.4 ft/s
- Vtheta2 = 10.478 ft/s
- Ctheta2 = 1279 ft/s
- U2 = 1289.5 ft/s

Stage 2 Pitch

- Alpha1 = 19.863 degrees
- Beta1 = 36.801 degrees
- V1 = 1462.3 ft/s
- C1 = 1244.9 ft/s
- Cx1 = 1170.9 ft/s
- Vtheta1 = 876 ft/s
- Ctheta1 = 423 ft/s
- U1 = 1299 ft/s
- Beta2 = 5.4017 degrees
- Alpha2 = 53.196 degrees
- V2 = 1032.2 ft/s
- C2 = 1715.3 ft/s
- Cx2 = 1027.6 ft/s
- Vtheta2 = 97.17 ft/s
- Ctheta2 = 1373.5 ft/s
- U2 = 1276.3 ft/s

Stage 3 Pitch

- Beta1 = 33.068 degrees
- Alpha1 = 26.196 degrees
- V1 = 1322.3 ft/s
- C1 = 1234.9 ft/s
- Cx1 = 1108.1 ft/s
- Vtheta1 = 721.48 ft/s
- Ctheta1 = 545.15 ft/s
- U1 = 1266.6 ft/s
- Beta2 = 3.6157 degrees
- Alpha2 = 54.557 degrees
- V2 = 929.44 ft/s
- C2 = 1599.6 ft/s
- Cx2 = 927.59 ft/s
- Vtheta2 = 58.614 ft/s
- Ctheta2 = 1303.2 ft/s
- U2 = 1244.5 ft/s

Stage 4 Pitch

- Beta1 = 37.799 degrees
- Alpha1 = 21.557 degrees
- V1 = 1318.9 ft/s
- C1 = 1120.5 ft/s
- Cx1 = 1042.2 ft/s
- Vtheta1 = 808.35 ft/s
- Ctheta1 = 411.71 ft/s
- U1 = 1220.1 ft/s
- Beta2 = 12.173 degrees
- Alpha2 = 47.434 degrees
- V2 = 936.13 ft/s
- C2 = 1352.8 ft/s
- Cx2 = 915.08 ft/s
- Vtheta2 = 197.39 ft/s
- Ctheta2 = 996.33 ft/s
- U2 = 1193.7 ft/s

Stage 5 Pitch

- Alpha1 = 7.4341 degrees
- Beta1 = 47.785 degrees
- V1 = 1404.7 ft/s
- C1 = 951.83 ft/s
- Cx1 = 943.83 ft/s
- Vtheta1 = 1040.3 ft/s
- Ctheta1 = 123.15 ft/s
- U1 = 1163.5 ft/s
- Beta2 = 29.63 degrees
- Alpha2 = 35.465 degrees
- V2 = 1004.3 ft/s
- C2 = 1071.8 ft/s
- Cx2 = 872.98 ft/s
- Vtheta2 = 496.53 ft/s
- Ctheta2 = 621.88 ft/s
- U2 = 1118.4 ft/s

Stage 6 Pitch

- Alpha1 = 3.4646 degrees
- Beta1 = 52.609 degrees
- V1 = 1301.2 ft/s
- C1 = 791.6 ft/s
- Cx1 = 790.1 ft/s
- Vtheta1 = 1033.8 ft/s
- Ctheta1 = 47.838 ft/s
- U1 = 1081.6 ft/s
- Beta2 = 44.861 degrees
- Alpha2 = 29.414 degrees
- V2 = 947.26 ft/s
- C2 = 770.79 ft/s
- Cx2 = 671.43 ft/s
- Vtheta2 = 668.19 ft/s
- Ctheta2 = 378.54 ft/s
- U2 = 1046.7 ft/s
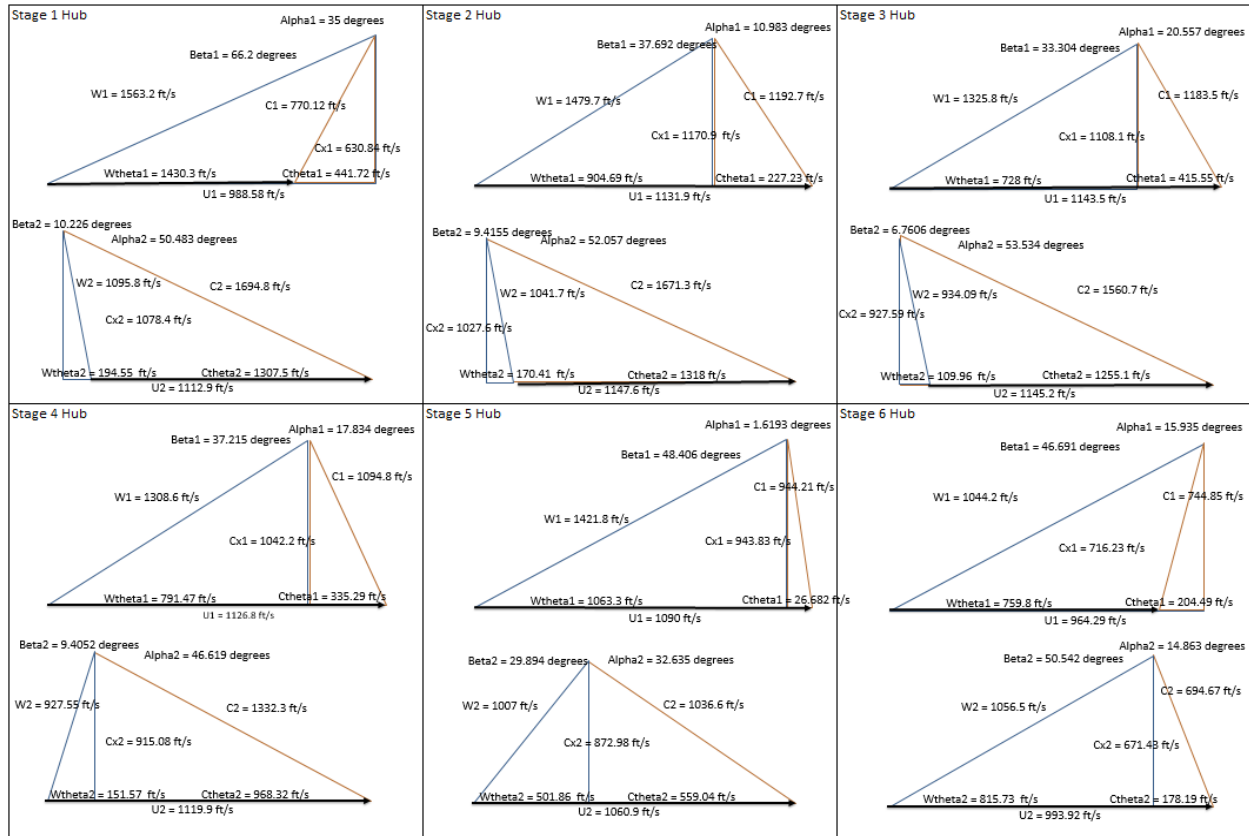
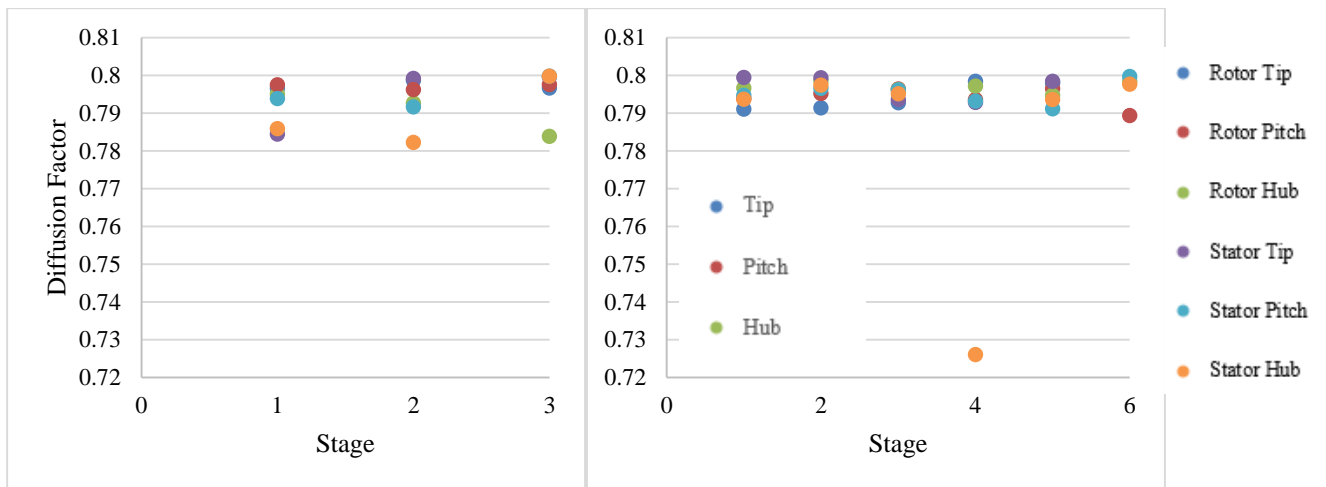**Figure 6.10** Compressor Velocity Diagrams at Hub, Pitch, and Tip

Figure 6.11a & 6.11b. Lieblein Diffusion Factors for a.) Fan & b.) Compressor
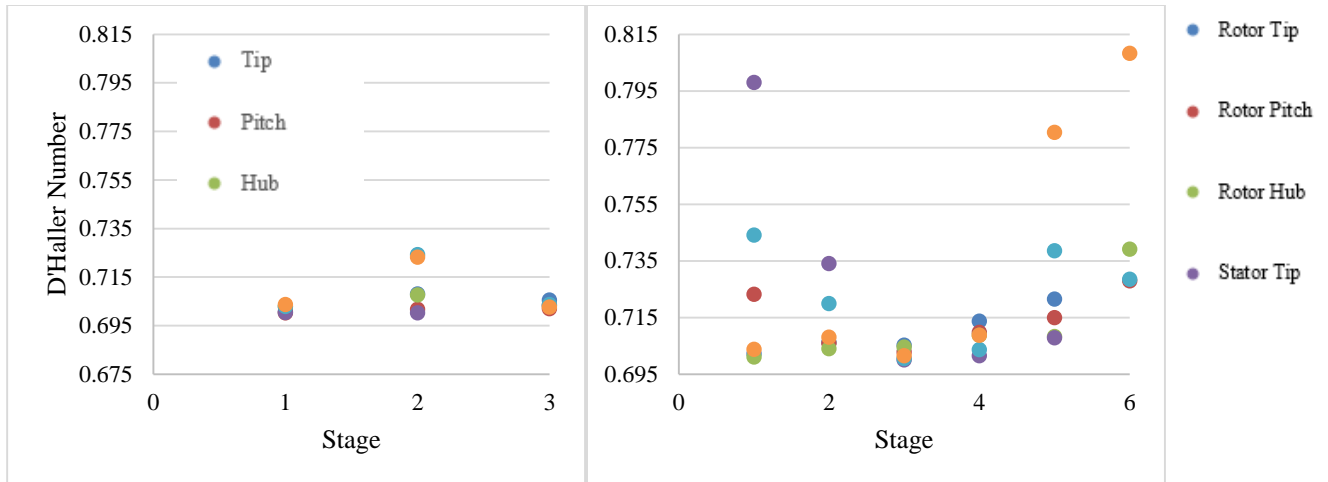
Figure 6.12a & 6.12b D'Haller Numbers for a.) Fan & b.) Compressor

Once a design was completed within the acceptable limits, the flow parameters at the tip and hub as well as blade information were finalized. The incidence and deviation of the rotors and stators were neglected, and the taper ratio was fixed at 1 (untapered blades).

B. Turbine Design

Referring to table 6.24 a two-stage HPT and two-stage LPT were selected that met the constraint on maximum stage loading coefficient. Six percent of the air was used for cooling the HP turbine disk.

	HPT	LPT
Delta T (R)	822.11	326.97
PR	6.85	2.25
Inlet Temp (T)	2520	1698
Inlet Pressure (psi)	245	35
Specific Work (BTU/lb)	196	123.7
AN^2 Limit	$5*10^{10}$	$4*10^{10}$
Relative Mach number limit	0.9	0.9
Minimum Blade Height	0.5	1
Maximum Loading Coefficient	2.2	2.2
Zweifel Coeficient	1.35	1.35

Table 6.23. Cycle Parameters and Design Specifications at Pitch Line

Based on the AN^2 limits and considerations for the relative Mach numbers in the fan and compressor, rotational speeds of 35000 RPM in the HPT and 17000 RPM in the LPT were selected.

In the preliminary design, the axial Mach number at the combustor exit was 0.2, and a constant axial velocity was assumed. The preliminary design was initiated and the stage flow coefficients and loading coefficients at the pitch line were calculated by iterating on pitch radii and pitch line design.

	HPT		LPT	
Stage	1	2	1	2
PR	2.88	2.38	1.67	1.35
Loading Coefficient	2.00	1.31	2.10	1.61
Flow Coefficient	0.35	0.35	0.64	0.61
Reaction	0.50	0.51	0.53	0.40
Relative Mach	0.87	0.82	0.69	0.73
Axial Mach	0.20	0.22	0.25	0.26
Stator Inlet Flow Angle	0.00	54.74	26.34	47.41
Stator Exit Flow Angle	76.74	73.81	65.34	69.28
Rotor Exit Flow Angle	54.74	26.34	47.41	1.00
Pitch Line Radii (inch)	4.4	4.7	5.0	5.3

Table 6.24. Vector Diagram Summary at Pitch Line

A Zweifel number of 1.35 was assigned at the pitch line of each blade row, and the number of blades was calculated.

	HPT		LPT	
Stage	1	2	1	2
Mean Radii (inches)	4.55	4.85	5.16	5.42
Hub/Tip Ratio	0.82	0.69	0.56	0.48
Axial Chord (inch)	0.90	1.05	0.97	1.09
Stagger Angle (°)	61.41	41.88	32.34	35.65
Blade Chord (inch)	1.89	1.41	1.15	1.34
Aspect Ratio	1.00	1.70	3.00	3.50
Zweifel Number	1.35	1.35	1.35	1.35
Pitch	0.25	0.22	0.34	0.34
Blade Count	114	142	94	100

Table 6.25. Rotor Blading Parameters (Pitch Line Average)

	HPT		LPT	
Stage	1	2	1	2
Mean Radii (inch)	4.40	4.70	5.01	5.31
Hub/Tip Ratio	0.88	0.77	0.62	0.50
Axial Chord (inch)	0.52	0.82	0.83	0.94
Stagger Angle (°)	38.10	59.67	36.45	33.58
Blade Chord (inch)	0.66	1.63	1.03	1.13
Aspect Ratio	1.10	1.50	2.80	3.75
Zweifel Number	1.35	1.35	1.35	1.35
Pitch	1.51	1.47	1.22	1.59
Blade Count	19	20	26	21

Table 6.26. Stator Blading Parameters (Pitch Line Average)

With the axial Mach numbers and the pitch radii determined, the flow path shown in Figure 6.27 was generated for the HP and LP turbines.
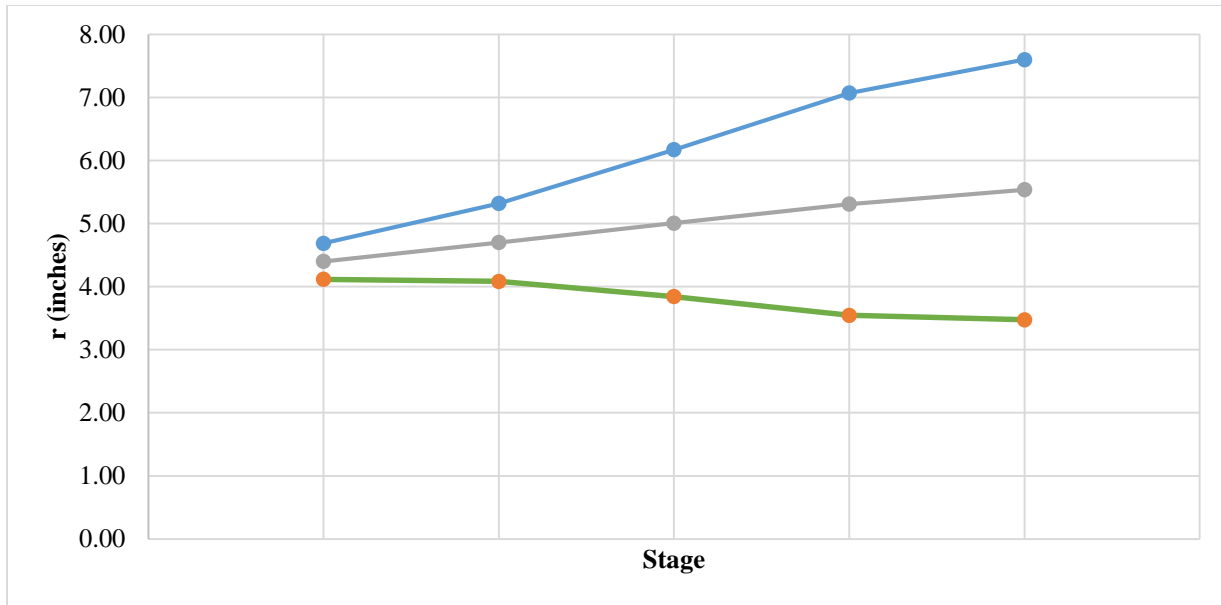
Figure 6.27. Flow Path for Turbine

From this point a free vortex approach to radial equilibrium was taken for the HPT, and the degree of reaction, loading coefficients, and flow coefficients were calculated. The reaction at the hub at each stage was acceptable. Since free vortex is not a valid approach for the LPT, the Carmichael and Lewis equation was applied [5].

$$Cu1 = a \times r - b/r \qquad\qquad [6.1]$$

$$Cu2 = a \times r + b/r \qquad\qquad [6.2]$$
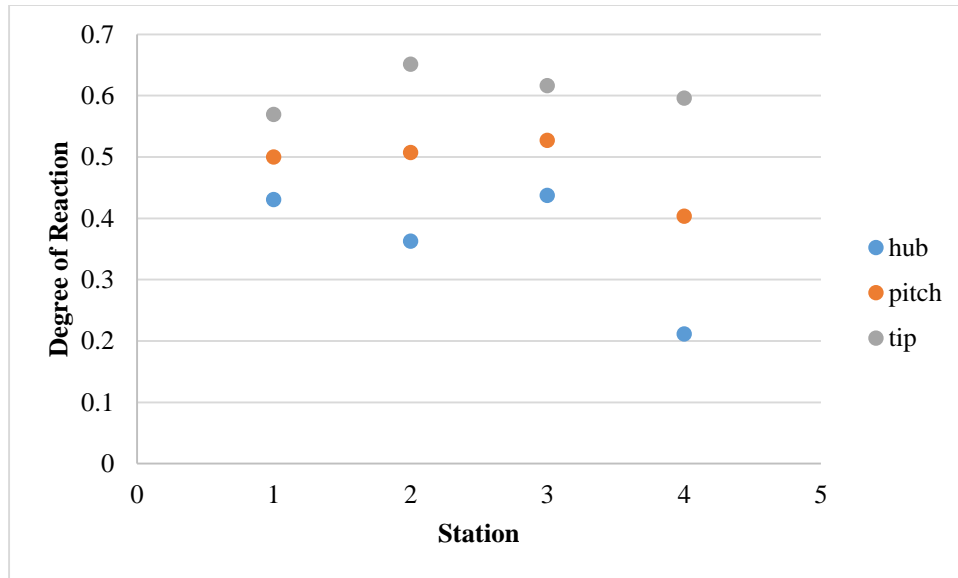
Figure 6.28. Degrees of Reaction for the HPT (Stations 1 and 2) and LPT (Stations 3 and 4)
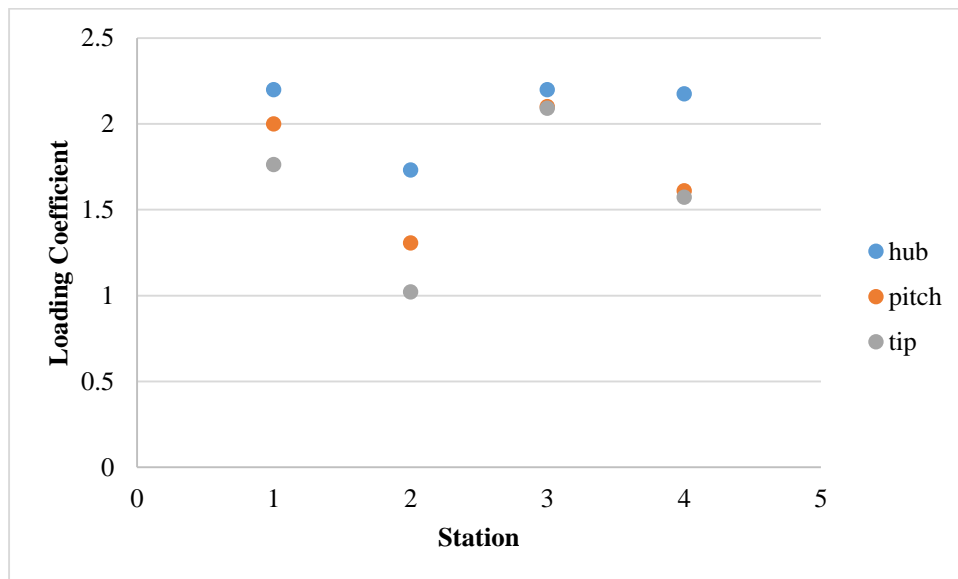
Figure 6.29. Loading Coefficients f for the HPT (Stations 1 and 2) and LPT (Stations 3 and 4)
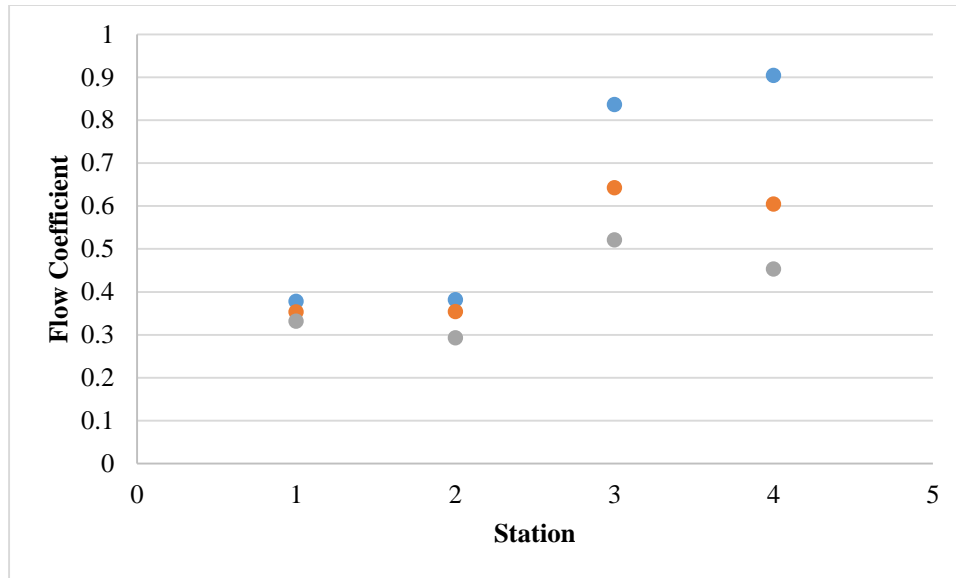
Figure 6.30 Flow Coefficients for the HPT (Stations 1 and 2) and LPT (Stations 3 and 4)

With this information, velocity triangles were generated at the hub, pitch, and tip locations. A hand set of calculations for each has been provided at the end of this section as well.
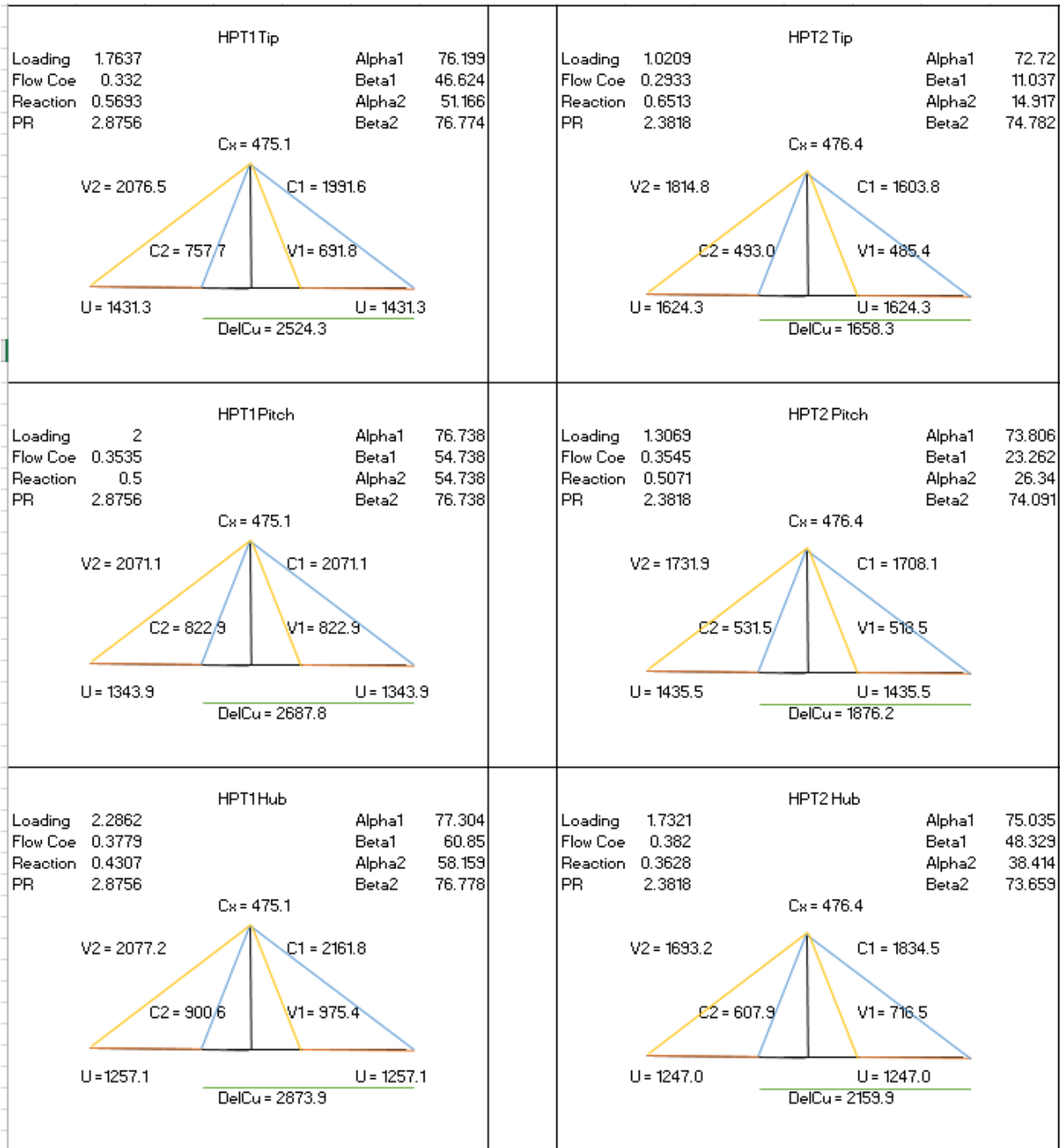
Figure 6.31 HPT Velocity Diagrams at Hub, Pitch, and Tip
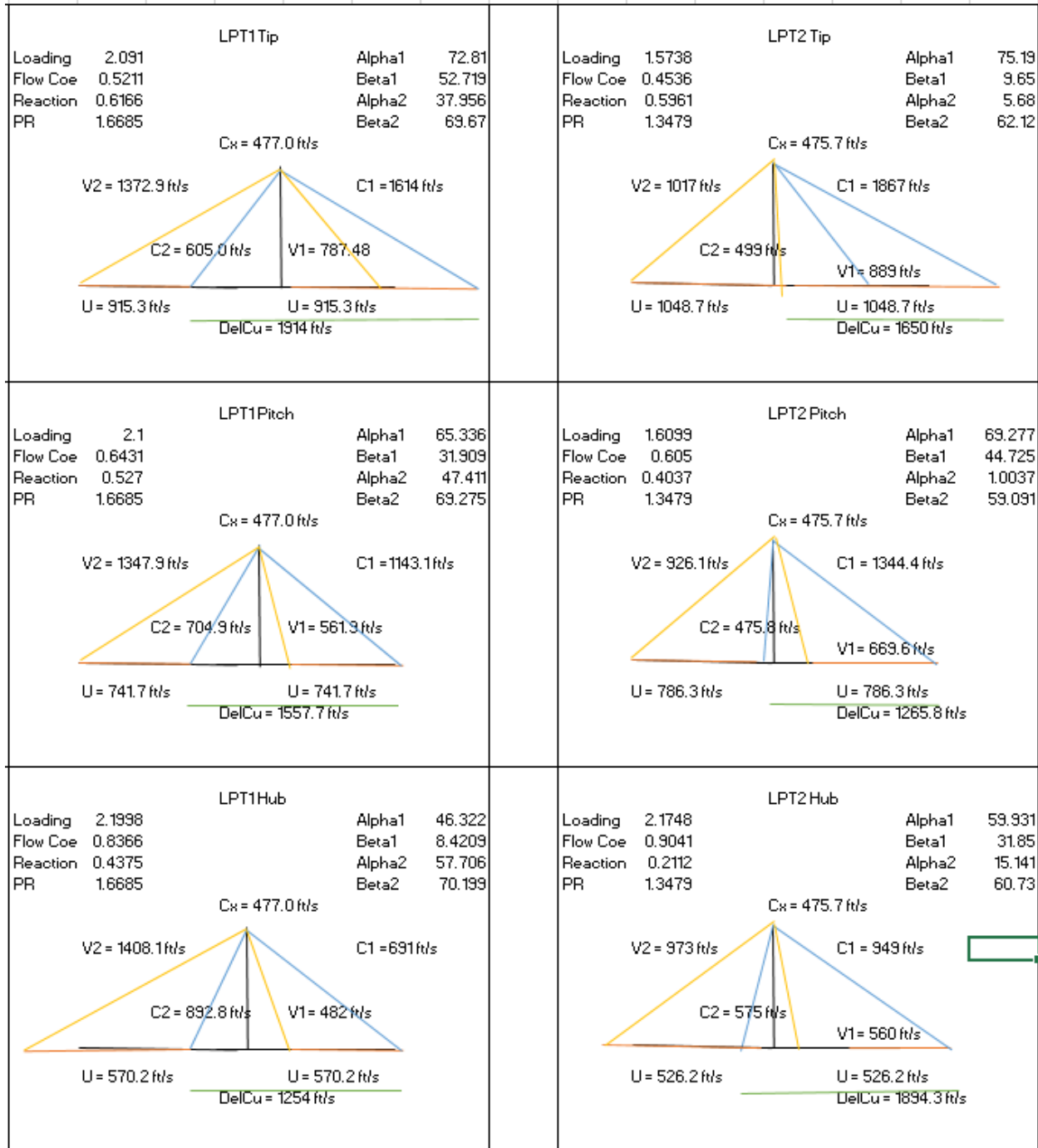
Figure 6.32. HPT Velocity Diagrams at Hub, Pitch, and Tip

$\omega = 17000$ RPM

$r = 4.24$ in

$U = \omega \times \frac{\pi}{180} \cdot \frac{r}{12}$

$U = 1296.1$

$M_{ax} = .51$

$C_x = 630.8$

$T_s = 636.80a$

$a = \sqrt{\gamma RT} = 1236.9$

$\alpha_1 = 5°$ (assumed)

Loading $= .9 \times U = \Delta C_u = 1168.2$

Figure 6.33. Compressor Hand Calculation

other values calculated from trig

$\omega = 35000 \ RPM = 3665.2 \ \frac{rad}{s}$

$r = 4.4 \ in$

$U = 1343.9 \ \frac{ft}{s}$

$M_{ax} = .2$

$C_x = 475.11 \ \frac{ft}{s}$

$Loading = 2 = \frac{\Delta C_u}{U}$

$\Delta C_u = 2 \cdot 1343.9 \frac{ft}{s} = 2687.8 \ \frac{ft}{s}$
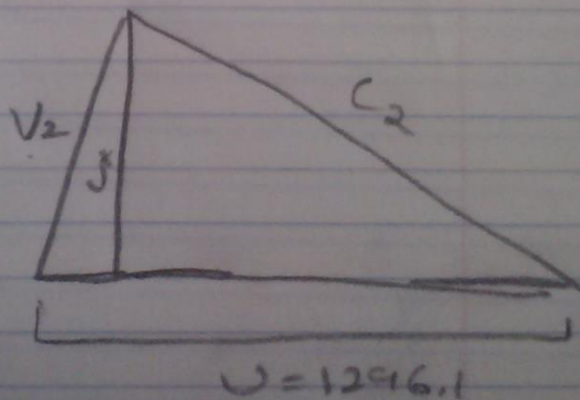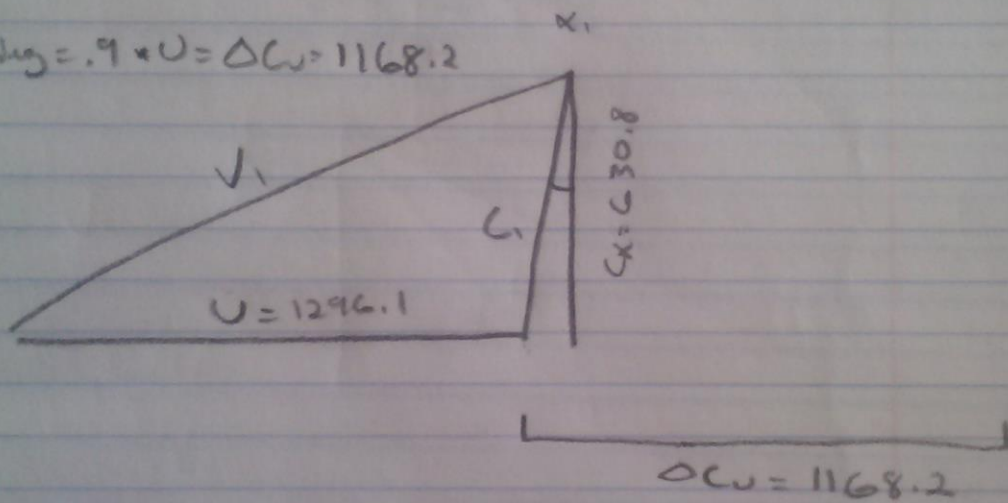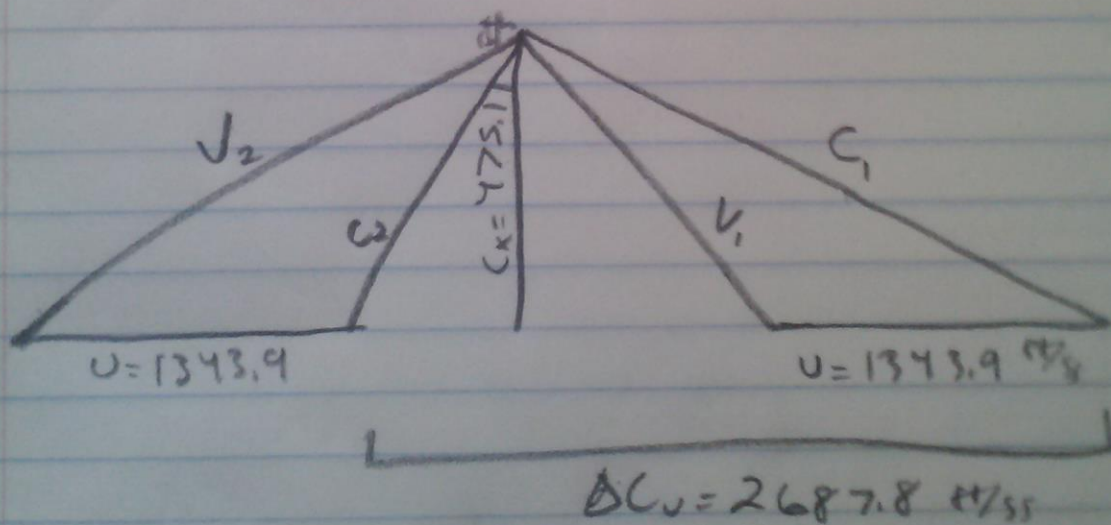
other values calculated from trig

Figure 6.34. Turbine Hand Calculation

VII.   Combustor Design

A. Combustor Concept

Recent developments in combustor technology have made lean burning combustors feasible for use in aviation engines, called LPP (Lean, Pre-mixed, Pre-vaporized). This concept has superseded traditional designs in many modern engines. Although less stable than traditional combustors, lean burning combustors have relatively lower NOx emissions, lower noise, and lower engine fuel burn. One example of this concept employed is the TAPS II combustor used in the GEnx and LEAP commercial aviation engines. It was developed alongside a NASA/FAA initiative for a clean combustor, compared to legacy technology. According to [12], the FAA has issued goals for combustor technology through 2025. These are listed in Table 7.1.

	N+1 (2015) Conventional Configuration Relative to 1998	N+2 (2020-25) Un-conventional Configuration Relative to 1998	N+3 (2030-2035) Un-conventional Configuration Relative to 1998
Noise	-32 dB	-42 dB	-71 dB
LTO NOx Emissions	-60 %	-75 %	Better than -75 %
Aircraft Fuel Burn	-33 %	-50 %	Better than -70 %

Table 7.1. FAA Clean Program Goals [12]

In addition, recent breakthroughs in additive manufacturing allow more advanced swirler and combustor liner designs. Because of this, effusion cooling has become cost-effective. Effusion cooling (small holes throughout the liner) extends the life of the engine with respect to traditional film cooling because it reduces thermal stresses compared to traditional film cooling.

The BC 4000 design will be utilizing a lean-burning combustor due to the maturation by 2025 of the technology and the life-cycle longevity it provides. Other military-grade engines, such as the Pratt and Whitney F119 use other emissions reducing concepts such as TALON [13],

pointing to increased attention to emissions and engine life cycle to the military. Also, due to recent major engine development programs in the commercial sector, it's believed that commercial aviation engine design will drive military engine design in the decades to come.

B. Combustor Inlet Conditions

Table 7.2 presents the flight conditions at which the combustor will be designed for. Design point is taken at takeoff because it represents the maximum power condition that the combustor section will see. All of these conditions are taken from the GasTurb cycle (refer to V.)

	$P_{3,0}$ (atm)	$T_{3,0}$ (°R)	Mass Flow (lbm/s)	Fuel-Air Ratio	$T_{4,1}$ (°R)
Takeoff*	**40.4**	**1,697**	**28.7**	**0.015**	**2,546**

Table 7.2. Engine Parameters

Using incompressible flow theory, the conditions leading into the pre-diffuser are calculated and presented in Table 7.3.

Speed of Sound, $a_{3,0}$ (ft/s)	2021
Density, $\rho_{3,0}$ (slug/ft^3)	0.029
Area, $A_{3,0}$ (ft^2)	0.06
Mach Number	0.26
Dynamic Pressure, $q_{3,0}$ (kPa)	565
Static Pressure, $p_{3,0}$ (kPa)	28.6

Table 7.3. Inlet Conditions at Takeoff to Combustor – SI Units

C. Diffuser Design & Combustor Sizing

To correctly size the combustor, the diffuser design and performance must be determined, as well as the passage flow conditions and velocities, according to the Lebvefre design method [11] and Mohammed et. al [15]. In this section, only the cold flow will be used for sizing purposes. The total pressure loss allowed for the combustor section is 5.6% of the compressor exit

pressure, from the cycle (V.). In addition, <u>4% has been reserved for the pressure drop across the</u> <u>swirlers and liners into the combustion zone.</u>

1. Aerodynamic Diffuser

The aerodynamic diffuser (or pre-diffuser) serves three primary purposes in the design of a combustor: to decrease the air velocity from the compressor section, recover some static pressure while decreasing the velocity, and help create an even air flow distribution before combustion occurs. The typical design tradeoff is to balance the length of the pre-diffuser with a low enough expansion angle to prevent separated flow along the wall.

Equations 7.1 through 7.8 were used to generate the performance of the aerodynamic diffuser, taken from Lebvebre [11] and Mohammed et. al [15]. Figure 8.3b was referenced for the nozzle loss coefficient calculation. Figure 7.3a was used to confirm there was no separation along the wall of the diffuser.

$$C_{p,ideal} = 1 - \frac{1}{AR^2} \qquad\qquad [7.1]$$

$$C_p = \eta \times C_{p,ideal} \qquad\qquad [7.2]$$

$$\left(L/_W\right) = \left(AR/_{1.044}\right)^{1/0.38859} - 0.26 \qquad\qquad [7.3]$$

$$\tan\theta = \frac{(AR-1)}{2(L/_W)} \qquad\qquad [7.4]$$

$$p_{3,1} = C_p \times q_{3,0} + p_{3,0} \qquad\qquad [7.5]$$

$$u_{3,1} = \frac{u_{3,0}}{AR} \qquad\qquad [7.6]$$

$$q_{3,1} = \frac{1}{2}\rho u_{3,1}{}^2 \qquad\qquad [7.7]$$

$$P_{3,1} = p_{3,1} + q_{3,1} \qquad\qquad [7.8]$$

Table 7.4 presents the performance of the aerodynamic diffuser with the variables calculated in Equations 7.1 through 7.8.

AR	2
η	0.85
L/W	5.07
2θ (degrees)	11.27
$\Delta P/P$ (%)	**0.5**

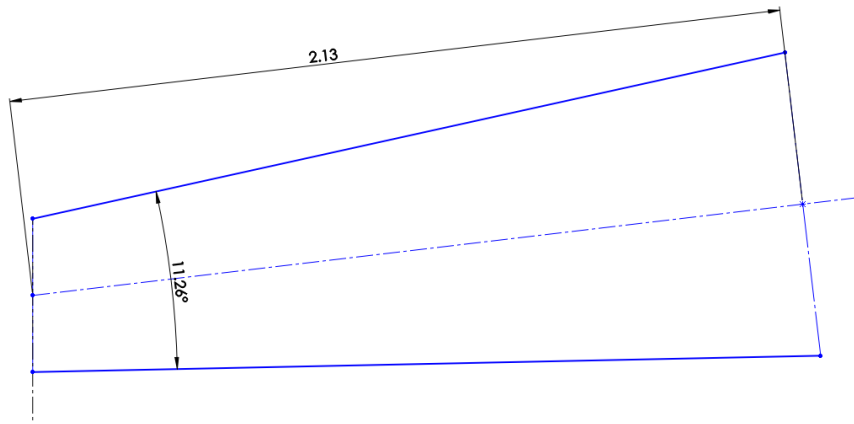**Table 7.4.** Aerodynamic Diffuser Design Quantities
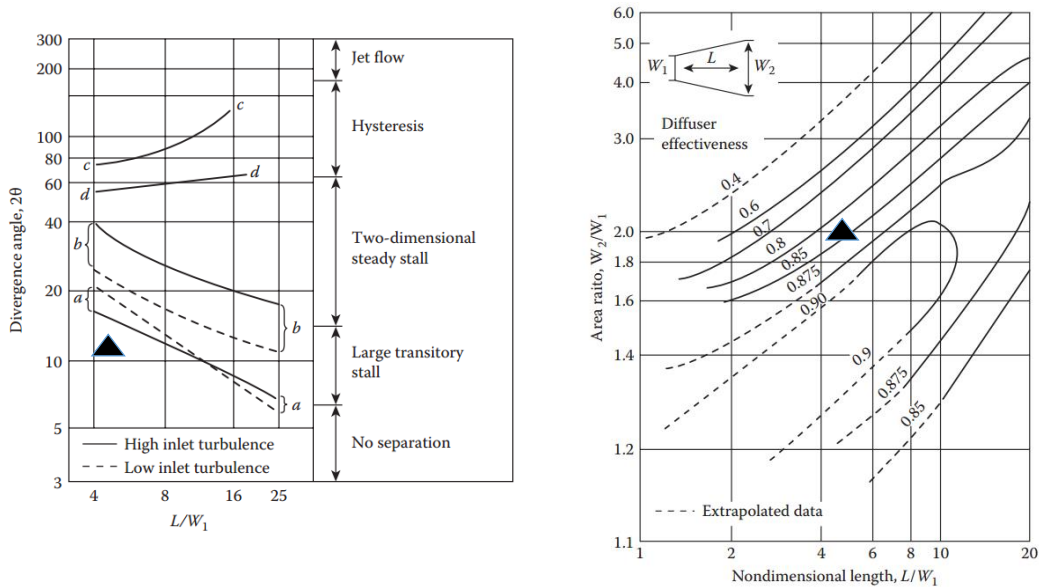

Figure 7.2. Aerodynamic Diffuser Design

Figure 7.3. a.) Flow Regime Determination, **b.)** Nozzle Effectiveness [11]

2. Combustor Sizing

In sizing the combustor, there are two main design philosophies. One is the pressure method, which serves to calculate the size required based off of pressure differentials [11]. This method, although very accurate, is difficult to achieve in preliminary design. The second is the velocity method [11], which refers to previous engine designs for sizing. This design will be using the velocity method, based on available literature such as Mohammed [15]. In sizing the combustor, Mohammed et al. [15] believe that the range of values for the passage velocity and dome velocity should be within the range presented in Table 7.5. The actual design quantities are presented as well.

	Assumption Range	Design Value
V_{dome}[†] (ft/s)	23-39	26.2
$V_{passage}$ (ft/s)	115-197	164

Table 7.5. Velocity Method Design Quantities [15]

Because this design will be using a lean burning combustor, the equivalence ratio needed in the primary zone will be lean. The flammability limit of JP-6 fuel is around 0.5 [11]. Because of this, the design point will be a <u>primary equivalence ratio of around 0.625.</u> For this to occur, the mass flow percentages were calculated to be 32%, 32%, and 36% for the inner, outer and dome flow passages, respectively. Figure 7.4 summarizes these results.
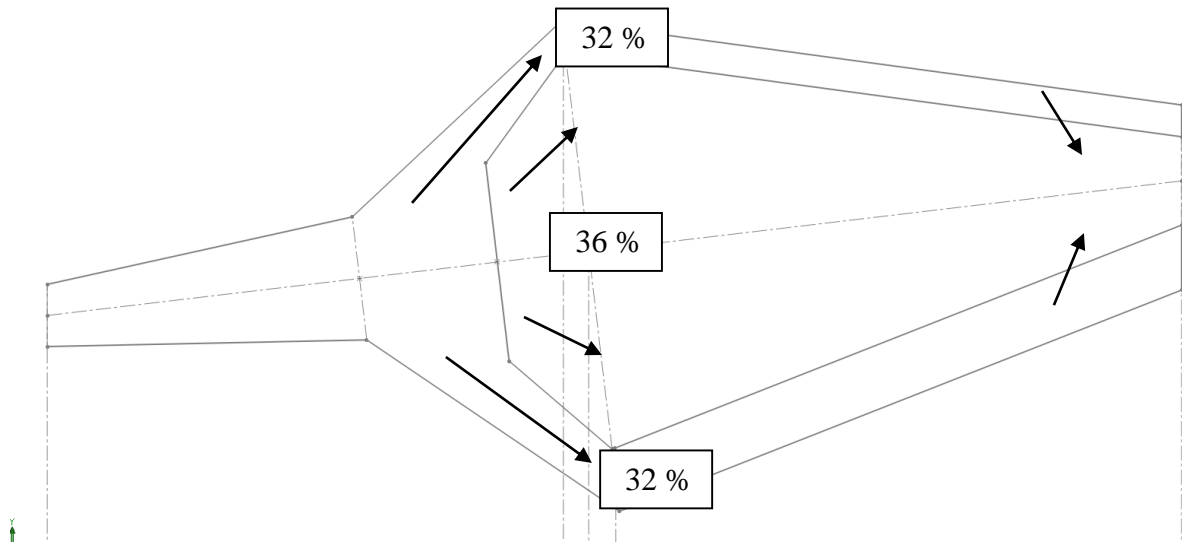

[†] Cold Flow Condition

Figure 7.4. Passage Mass Flow Quantities (% of entrance mass flow)

First, two areas are calculated: total passage area [7.9] and dome area [7.10]. Total passage area is shown to be the sum of half of the inner and outer passage areas [7.11] due to the total passage mass flow rate being divided equally between the two. This assumption follows from the assumed constraint that the inner and outer passages will have the same annular area. A reference area representing the total annular area of the combustor station was calculated [7.12] for use in calculating geometric values [15].

$$A_{P,total} = \frac{W_{P,t}}{\rho_3 V_{P,t}} \qquad\qquad [7.9]$$

$$A_D = \frac{W_D}{\rho_3 V_D} \qquad\qquad [7.10]$$

$$A_{P,total} = \frac{A_{P,i}}{2} + \frac{A_{P,o}}{2} \qquad\qquad [7.11]$$

$$A_{ref} = A_{P,total} + A_D \qquad\qquad [7.12]$$

Next, the 2D axisymmetric geometry values are calculated from the annular areas. These values include pitch radii ($R_{P,P}$ and $R_{P,D}$) and heights of each passage (H_P) and the dome (H_D). They are related in [7.13] and [7.14].

$$H_P = \frac{A_P}{2\pi R_{P,P}} \qquad [7.13]$$

$$H_D = \frac{A_D}{2\pi R_{P,D}} \qquad [7.14]$$

To begin, an "overall passage height" was defined as a function of reference area, dome pitch radius, and dome height [7.15]. This represents the total height of the passages. Using the constraint that the inner and outer passages will have the same area, [7.16] and [7.17] formed a set of linear equations that could be solved for inner and outer passage heights.

$$H_{P,overall} = \frac{A_{ref}}{2\pi R_{P,D}} - H_D = H_{P,inner} + H_{P,outer} \qquad [7.15]$$

$$r_{P,inner} \times H_{P,inner} = r_{P,outer} \times H_{P,outer} \qquad [7.16 \text{ \& } 7.17]$$

To simplify the solution of this system, a dome pitch radius was assumed to be 9.46 (cm), which was along the centerline of the pitch radius of the combustor. Using [7.14], dome height was calculated. Both inner and outer passage pitch radii were given assumed values iteratively and solved while simultaneously generating a sketch model to check the design feasibility of the calculated geometry.

The combustor length was then calculated by assuming a combustor length to dome height ratio [7.18]. According to Mohammed et al. [15], for an RQL combustor, this value should be 2. However, this number was subtracted from because this design uses an LPP, and materials technology should allow for shorter combustors in 2025. In addition, a correlation for the number of swirl cups in the annulus is calculated according to [15] in equation 7.19. All combustor

geometry values are summarized in Table 7.6. A sketch model of the combustor can be found at the end of this section.

$$\frac{L}{H_D} = 1.5 \qquad\qquad [7.18]$$

$$No.\ Cups = \frac{2\pi \times R_{P,D}}{H_D} \qquad\qquad [7.19]$$

Passage Area (in^2)	18
Dome Area (in^2)	63
Dome Height (in)	2.7
Dome Pitch Radius (in)	3.7
Outer Passage Height (in)	0.22
Inner Passage Height (in)	0.54
Combustor Length (in)	4.05
Number of Swirl Cups	9

Table 7.6. Combustor Design Geometry

3. Dump Diffuser Performance

Once the areas and passage sizes were calculated for the combustor geometry, it is possible to calculate pressure loss in this section from equation 7.20, according to Mohammed et al. [15]. It was found that the <u>pressure loss in the dump diffuser was about 1.1% of the incoming pressure.</u>

$$\Delta P_{Dump} = (P_{3,2} - p_{3,2}) * \left(1 - \left(\frac{A_{3,1}}{A_{3,2}}\right)^2\right) \qquad\qquad [7.20]$$

D. Swirler Design and Flame Generation

One of the unique qualities in a turbofan engine is the ability to continuously auto-ignite the fuel-air mixture without the aid of a spark during normal operating conditions. It's an important design feature in the combustor, and it's accomplished by employing a region of toroidal flow reversal that entrains and recirculates the hot gases back to the dome plane to mix with the incoming fuel/air mixture. This reversal can be seen in figure 7.5. This flow is produced by a

swirler, in which the air enters radially or axially and turned in order to convert axial momentum into radial momentum.

In this design, the swirler will be an axial-radial, with the axial interior supporting the pilot flame region, and the radial in the exterior, supporting the premixing flame zone. The complete design is not in the scope of this report, but the effective areas of each are calculated via equation 7.21.

$$\dot{m}_{flow} = \left[A_{eff}\right] \times \sqrt{2\rho\Delta P} \qquad [7.21]$$

In the preceding sections, it was found that the dump and aerodynamic diffusers had pressure losses of 1.6 percent combined. Therefore, the <u>pressure loss across the combustion section will be 4% of the incoming pressure.</u> The effective areas are then calculated for each single swirl cup and presented in Table 7.7.

	Type	Effective Flow Area (in^2)	Percent of the Mass Flow at 3,0 (%)
Main Swirler (Cyclonic Mixers)	Radial	0.21	28
Pilot Swirler	Axial	0.06	8

Table 7.7. Swirler Constraints

E. Fuel Supply

The fuel used will be JP-6 for the engine, and must be supplied to each swirler for adequate mixing. The configuration is presented in Figure 7.5.
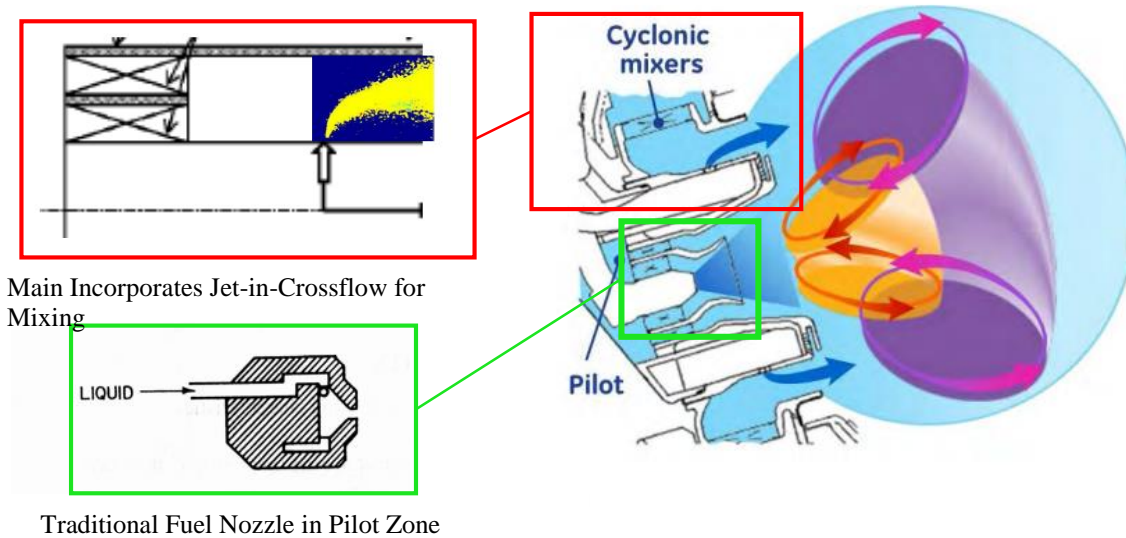
Main Incorporates Jet-in-Crossflow for Mixing

Traditional Fuel Nozzle in Pilot Zone

Figure 7.5. LPP Swirler Fuel Injection Configuration

4. Pilot

The pilot fuel nozzle mixes with the axial swirler in a partially premixed fashion. It provides the region of flame stabilization for the hot gases. Figure 7.6 provides an example of the configuration.

5. Main

The main swirler is located outside of the pilot swirler, and consists of a series of jet flows. Each swirler vein is represented as a "jet in crossflow." The jet must penetrate the air enough so that the fuel is adequately premixed. Also, this allows the jet to travel downstream into the hot gases without attaching to the wall.

F. Combustor Schematic

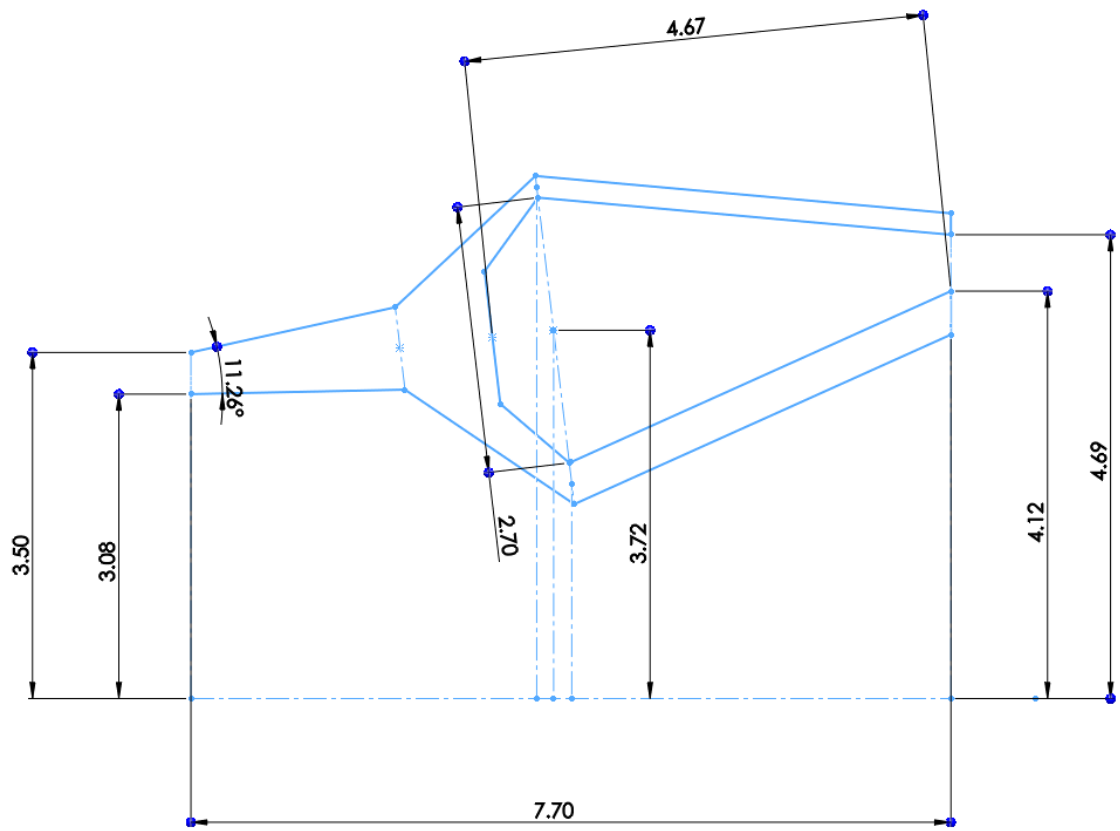A schematic of the combustor design is presented in Figure 7.6.

Figure 7.6. Combustor Final Design (inches)

VIII.   Nozzle Design

A comparative analysis was conducted to evaluate the engine gross thrust that is obtained when the afterburner is on at Mach 1.3 dash and at take-off with a convergent-divergent vs a convergent nozzle. The results of these are summarized in Tables 8.1 and 8.2.

	Takeoff	Supersonic Dash
Inlet P_{total} (psia)	36.68	18.543
$P_{ambient}$ (psia)	14.696	2.720
Inlet T_{total} (Rankine)	3,025	2,450
P/Pt	0.4	0.147
T/Tt	0.81	0.649
Exit Mach Number	1.25	1.9
Gross Specific Thrust (ft/s)	**2,922**	**3,616**

Table 8.1. Flow Conditions in Convergent-Divergent Nozzle

	Takeoff	Supersonic Dash
T* (Rankine)	2,629	2,129
$P_{critical}$ (psia)	19.99	10.11
ρ* (lb/ft^3)	4.44e-6	2.77e-6
V* (ft/s)	2,422	2,179
Gross Specific Thrust (ft/s)	**2,826**	**3,345**

Table 8.2. Flow Conditions in Convergent Only Nozzle

If a convergent nozzle was used, the gross thrust would be reduced by 3% during one-minute-long takeoff and 8% at one-minute-long Mach 1.3 dash. This comparison suggests that the added complexity of using a convergent-divergent nozzle might not be justified during these short flight periods of afterburning flight.

Because of the use of the afterburner, a variable nozzle is still necessary. The following equation was used to calculate the convergent nozzle exit, or nozzle throat area, for each flight condition.

$$\dot{m} = \frac{A p_t}{\sqrt{Tt}} \sqrt{\frac{\gamma}{R}} M \left(1 + \frac{\gamma-1}{2} M^2 \right)^{\frac{-(\gamma+1)}{2(\gamma-1)}} \qquad [8.1]$$

Rearranging to solve for area:

$$A = \frac{\dot{m}\sqrt{T_t}}{p_t} \frac{1}{\sqrt{\gamma/R}} \frac{1}{M}\left(1 + \frac{\gamma-1}{2}M^2\right)^{\frac{(\gamma+1)}{2(\gamma-1)}}$$

[8.2]

Then, the diameter can be calculated with the following

$$R = \sqrt{\frac{A}{\pi}}$$

[8.3]

Table 8.5 shows the Area of the exit for a convergent nozzle, or the required throat area if a convergent divergent nozzle was used.
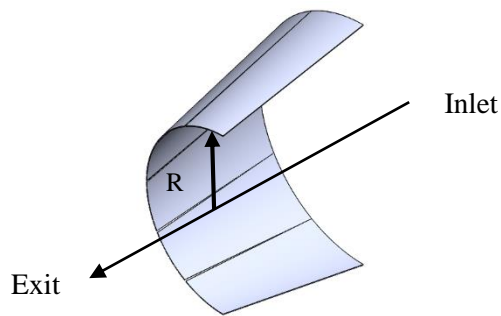
Figure 8.1. Schematic of Nozzle

	Thrust (lbf)	Area$_8$ (in^2)
Takeoff	4,003	131.66
Top of Climb	774	80.66
Cruise	637	80.66
Supersonic Dash	1,500	115.68
Loiter	1,234	80.66

Table 8.5. Geometry of Nozzle at Each Flight Condition

IX. Engine Overview

A. Cross Section/Flow Path

The engine cross section sketch in Figure 9.1 refers to the flow-paths generated in the preceding sections. Actual flow-paths of the major components are presented in Figures 6.5 and 6.27 for the fan and compressor, and 7.6 for the combustor.
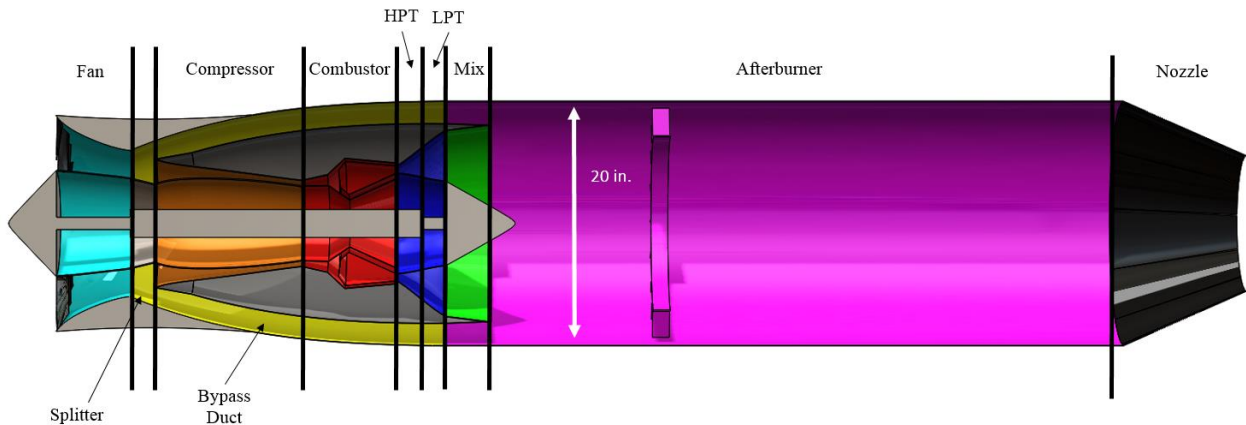
Figure 9.1. Sketch of Engine Cross Section

B. Materials

During the original advent of the J85 engine during the late 1980's, materials science had not yet strayed away from metals to newly formed composites and ceramics. Therefore, many of the materials used in the original engine were heavier and less heat resistant than their more advanced counterparts today. It is imperative to improve upon the materials that were used in the old engine. This section provides an overview of the baseline materials used for each major section of the engine and the new materials that are thought to take their place by 2025.

1. Baseline Materials (J85)

The combustion chamber is the hottest region of the engine, and therefore needs materials that can withstand this high heat load. During the 1980's and until the development of N5, Inconel 718 was the material of choice for most combustors. For this reason, it is assumed that the original combustion chamber was completely Inconel based. Introduction of the material named "N5" started in the late 1980's (~1989) and was widely used for sections of engines that required high heat capabilities after its full market introduction. Prior designs that used Inconel or N4 (pre-cursor to N5), were replaced with the newer N5 because of its increased resilience to heat loads. Likewise, N5 was subsequently replaced by the newly developed N6 in 1994. However, N6 had many manufacturing concerns, so N5 continued to be the material of choice for engine designers through the end of the 20th century. Today, N5 is still widely used on older engines and parts. Figure 9.2 provides an overview on material advancement through the early 21st century. Table 9.1 provides an overview of the original materials used in the J85

Engine Section	Material
Fan	n/a (DNE)
Compressor Blades	Titanium Alloy
Compressor Disk	Inconel 718
Compressor Stators	Inconel 718
Combustion Chamber	Inconel 718
Turbine Blades	N5
Turbine Disk	Inconel 718
Turbine Stators	N5
Internal Case (Not Nacelle)	Inconel 718
Nozzle	n/a

Table 9.1. J85 Material Breakdown
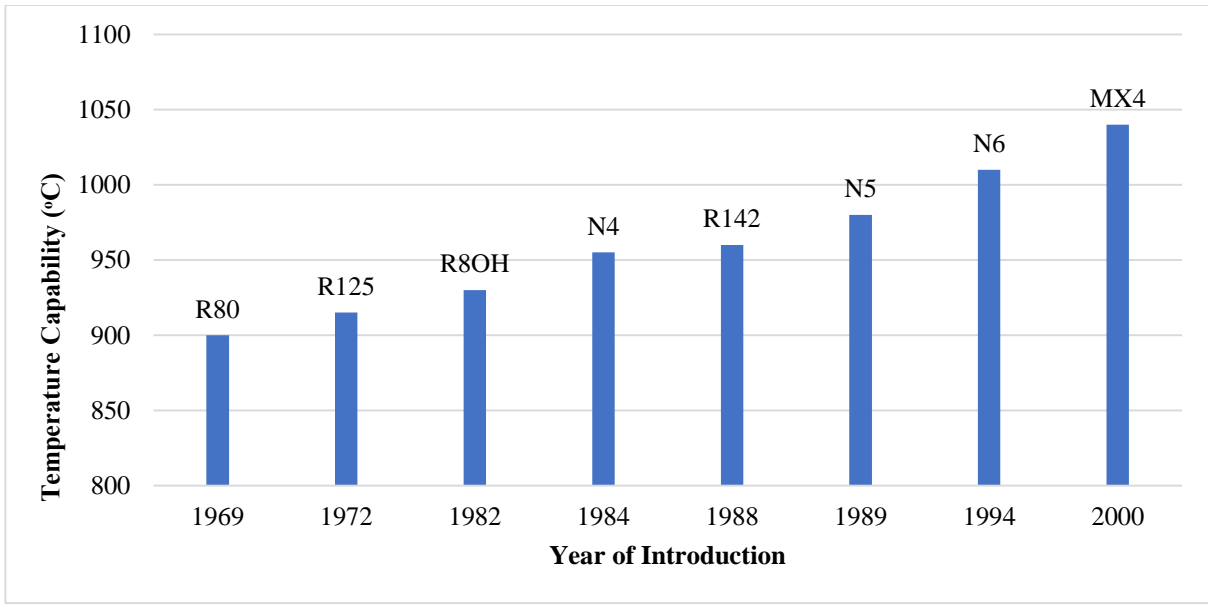
Figure 9.2. Historical Trend – Turbine Blade Alloy Temperatures

2. *Improved Materials (Bearcat 4000 Engine)*

The new compressor, combustion chamber, and core sections will have a dramatic reduction in size and weight because of the incorporation of bypass air in the new engine in addition to improved materials. The former 20-inch nacelle will be kept, resulting in a subsequent reduction in diameter of each component in comparison to its original counterpart. For reference, Table 9.2 shows the projected materials that will form the bulk of the redesigned engine.

Contemporary engines were used to provide feasibility and justification for incorporating newly developed materials. In the compressor sections, polymer matrix composites will replace the formerly used titanium alloys in stages one through three. This same design will be used in the GE-9X, which will begin full production in 2020. Carbon weaves are the lightest material that can feasibly be used that is known of today, and although their heat resistance is questionable, the beginning stages of the compressor don't see a large amount of heat.

In the combustion chamber, recent breakthroughs in ceramics, as well as increased manufacturing capabilities of these materials, have given designers more flexibility and access to

a higher domain of combustor and turbine entry temperatures. A result of this is the decreased need of cooling air and film cooling along the combustor walls, decreasing the overall length of the combustor and dramatically decreasing the overall weight.

The same materials developed for use in the combustion chamber will also be used in the turbine stators: ceramic matrix composites. These materials can withstand very high temperatures without the need for cooling. This will provide a large reduction in weight in comparison to the original engine. The blades will be titanium aluminide due to a precedent of reliable manufacturing techniques and the ability to handle the high aeromechanical loads.

Engine Section	Material
Fan	Polymer Matrix Composite
Compressor Blades	Titanium Alloy
Compressor Disk	Inconel 718
Compressor Stators	Inconel 718
Combustion Chamber	Ceramic Matrix Composite
Turbine Blades	Titanium Aluminide
Turbine Disk	Inconel 718
Turbine Stators	Ceramic Matrix Composite
Internal Case (Not Nacelle)	Inconel 718
Nozzle	n/a

Table 9.2. Bearcat Engine Materials Breakdown

C. Weight Estimation

Since the J85's development in the 1950's, the weight of gas turbine engine components has dropped considerably due to the use of advanced materials and lower part counts. For this reason, along with the fact that a bypass was implemented into the design, the Bearcat 4000 engine will have a much lower weight than the J85, even with the two engines being very close in overall physical size. For a quantitative estimate of the overall engine weight, a more advanced production engine with a similar bypass ratio was chosen, and its weight was scaled

based on inlet diameter cubed. For this assessment, the Pratt & Whitney F119 engine was selected, as it has an identical bypass ratio to the BC 4000, and is the most advanced low bypass engine with published size and weight data [16]. The weight estimate, along with a comparison of the J85, is laid out in Table 9.1.

PW F119			Bearcat 4000			J85		
Diameter (in.)	D^3 (in.^{3})	Weight (lbm)	Diameter (in.)	D^3 (in.^{3})	Weight (lbm)	Diameter (in.)	D^3 (in.^{3})	Weight (lbm)
46	97336	3900	17.6	5452	**218**	17.7	5545	396

Table 9.1. Engine weight Evaluation

X. Summary

The Bearcat 4000 engine has been presented as the replacement for the J85. It is an afterburning turbofan with a three stage fan and six stage compressor powered by a two stage HP turbine and two stage LP turbine. The afterburning turbofan met or exceeded all thrust requirements throughout the mission, with a 28% reduction in specific fuel consumption at cruise. A bypass ratio of 0.35 has resulted in a decreased engine core size, leading to an estimated 44% reduction in engine weight compared to the J85.

Appendix A – Gas-Turb Cycle Analysis
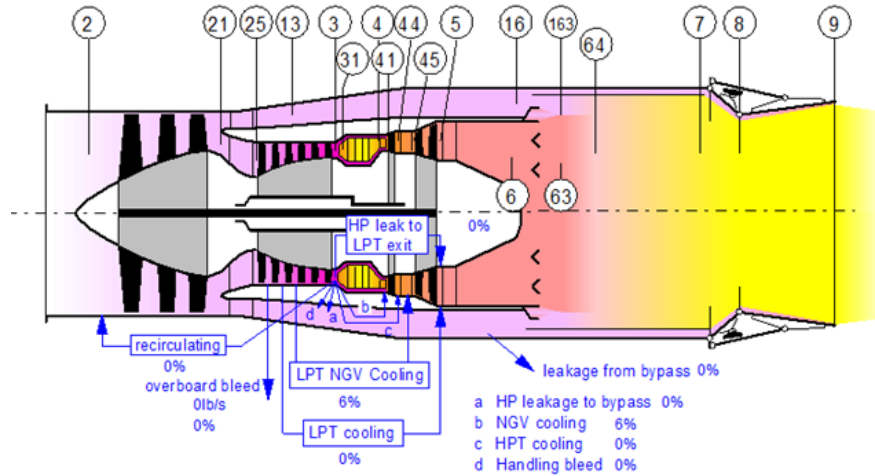
Figure A.1. Station Designation

Ambient Conditions	Takeoff (Design Point)	Cruise	Top of Climb	Supersonic Dash	Loiter
Altitude	**0**	35000	35000	40000	15000
Flight Mach Number	**0**	0.85	0.85	1.3	0.5
Temperature (°R)	**545.67**	429.85	429.85	416.97	492.18
Pressure (psia)	**14.696**	3.458	3.458	2.72	8.294
Thermodynamic Properties					
Ratio of specific heats for air	**1.4**	1.4	1.4	1.4	1.4
Ratio of specific heats for hot air	**1.3**	1.3	1.3	1.3	1.3
Fuel heating value (btu/lbm)	**18400**	18400	18400	18400	18400
Pressure Losses					
Inlet pressure drop (%)	**1**	1	1	3	1
Duct pressure drop (%)	**3.8**	4.3	3.6	3.8	4.3
Nozzle CD	**0.961**	0.965	0.975	0.959	0.962
Polytropic Efficiencies					
Fan	**0.89**	0.89	0.82	0.90	0.89
Compressor	**0.89**	0.89	0.88	0.89	0.89
High Pressure Turbine	**0.85**	0.85	0.85	0.85	0.85
Low Pressure Turbine	**0.89**	0.88	0.88	0.88	0.89
Sizing Parameters					
Corrected Airflow	**43.3**	43.3	43.3	43.3	43.3
Thrust Required	**4000**	635	762.15	1500	1230

Table A.11. GasTurb Inputs

1. Gas-Turb Outputs

Takeoff (AB=3025R)

Station	W lb/s	T R	P psia	WRstd lb/s				
amb		545.67	14.696		FN	=	4003.01 lb	
1	43.434	545.67	14.696		TSFC	=	1.6398 lb/(lb*h)	
02	14.594	545.67	14.696	33.000	P02/P1	=	1.00000	
12	5.108	545.67	14.129	12.013	P12/P1	=	0.96143	
2	43.434	545.67	14.549	45.000	WF Burner=		0.42159 lb/s	
13	11.261	767.21	40.974	4.912	s NOX	=	2.3252	
21	32.173	767.21	42.618	13.493	BPR	=	0.3500	
25	32.173	767.21	42.618	13.493	Core Eff =		0.4249	
3	30.243	1697.41	587.706	1.368	Prop Eff =		0.0000	
31	28.312	1697.41	587.706					
4	28.734	2600.00	564.198	1.676	P3/P2	=	40.395	
41	30.664	2546.20	564.198	1.770	P16/P6	=	1.05566	
43	30.664	1716.63	82.266		A63	=	431.60 in²	
44	30.664	1716.63	82.266		A163	=	31.44 in²	
45	32.595	1664.35	81.444	10.536	A64	=	463.04 in²	
49	32.595	1397.83	37.638		XM63	=	0.08525	
5	32.595	1397.83	37.638	20.893	XM163	=	0.29237	
6	32.595	1397.83	37.261		XM64	=	0.10000	
16	11.261	767.21	39.335		P63/P6	=	0.99000	
64	43.855	1242.75	37.091		P163/P16	=	0.99000	
7	20.528	3025.00	36.683		WF total =		1.82342 lb/s	
8	45.257	3025.00	36.683	43.786	A8	=	131.66 in²	
Bleed	0.000	767.21	42.618		CD8	=	1.00000	

Efficiencies:	isentr	polytr	RNI	P/P	P8/Pamb =		2.49614
Outer LPC	0.8700	0.8877	0.932	2.900	WLkBy/W25=		0.00000
Inner LPC	0.8700	0.8877	0.932	2.900	W_NGV/W25=		0.06000
HP Compressor	0.8500	0.8914	1.819	13.790	WHcl/W25 =		0.00000
Burner	0.9990			0.960	Loading =		100.00 %
HP Turbine	0.8800	0.8522	5.981	6.858	e444 th =		0.88028
LP Turbine	0.9000	0.8907	1.404	2.164	WLcl/W25 =		0.00000
Mixer	1.0000				WBHD/W21 =		0.00000
Reheat	0.9500			0.989	WF Reheat=		1.40183 lb/s
					XM64 =		0.10000
					XM7 =		0.16969

Figure A.2.

Top of Climb

Station	W lb/s	T R	P psia	WRstd lb/s				
amb		420.85	3.458		FN	=	774.02 lb	
1	18.260	481.79	5.547		TSFC	=	0.8823 lb/(lb*h)	
02	6.381	481.79	5.547	35.916	P02/P1	=	1.00000	
12	1.902	481.79	5.306	11.192	P12/P1	=	0.95645	
2	18.260	481.79	5.492	47.092	WF Burner=		0.18969 lb/s	
13	4.193	718.32	16.716	4.338	s NOX	=	1.4335	
21	14.067	718.32	17.477	13.920	BPR	=	0.2981	
25	14.067	718.32	17.477	13.920	Core Eff =		0.4996	
3	13.223	1644.71	255.588	1.354	Prop Eff =		0.5605	
31	12.379	1644.71	255.588					
4	12.569	2575.57	245.575	1.676	P3/P2	=	46.539	
41	13.413	2520.30	245.575	1.769	P16/P6	=	1.03632	
43	13.413	1698.19	35.856		A63	=	431.60 in²	
44	13.413	1698.19	35.856		A163	=	31.44 in²	
45	14.257	1644.47	35.530	10.500	A64	=	463.04 in²	
49	14.257	1371.22	15.795		XM63	=	0.08810	
5	14.257	1371.22	15.795	21.567	XM163	=	0.25176	
6	14.257	1371.22	15.627		XM64	=	0.10000	
16	4.193	718.32	16.195		P63/P6	=	0.99000	
64	18.449	1229.42	15.518		P163/P16	=	0.99000	
8	18.449	1229.42	15.207	27.450	A8	=	80.66 in²	
Bleed	0.000	718.32	17.477		CD8	=	1.00000	

Efficiencies:	isentr	polytr	RNI	P/P	P8/Pamb =		4.39765
Outer LPC	0.7885	0.8193	0.408	3.151	WLkBy/W25=		0.00000
Inner LPC	0.7885	0.8193	0.408	3.151	W_NGV/W25=		0.06000
HP Compressor	0.8310	0.8786	0.807	14.624	WHcl/W25 =		0.00000
Burner	0.9966			0.961	Loading =		215.78 %
HP Turbine	0.8807	0.8530	2.634	6.849	e444 th =		0.88109
LP Turbine	0.8911	0.8805	0.621	2.249	WLcl/W25 =		0.00000
Mixer	0.9000				WBHD/W21 =		0.00000
					far7 =		0.01039
HP Spool mech Eff 0.9900 Speed 35000 rpm					WBLD/W25 =		0.00000
LP Spool mech Eff 0.9900 Speed 20933 rpm					PWX	=	0.0 hp
					P16/P13 =		0.9688

Figure A.3.

Cruise (Throttle=93.6%)

Station	W lb/s	T R	P psia	WRstd lb/s			
amb		420.85	3.458		FN	=	636.97 lb
1	17.391	481.79	5.547				
02	5.808	481.79	5.547	32.694	TSFC	=	0.8353 lb/(lb*h)
12	2.080	481.79	5.337	12.172	P02/P1	=	1.00000
2	17.391	481.79	5.492	44.852	P12/P1	=	0.96208
13	4.586	676.80	15.433	4.989	WF Burner=		0.14779 lb/s
21	12.805	676.80	16.041	13.401	s NOX	=	0.9389
25	12.805	676.80	16.041	13.401	BPR	=	0.3582
3	12.036	1516.93	221.075	1.368	Core Eff =		0.4962
31	11.268	1516.93	221.075		Prop Eff =		0.5956
4	11.416	2333.34	212.228	1.677	P3/P2	=	40.254
41	12.184	2284.24	212.228	1.771	P16/P6	=	1.05845
43	12.184	1529.57	30.959		A63	=	431.60 in²
44	12.184	1529.57	30.959		A163	=	31.44 in²
45	12.952	1482.24	30.678	10.489	A64	=	463.04 in²
49	12.952	1241.66	14.119		XM63	=	0.08478
5	12.952	1241.66	14.119	20.859	XM163	=	0.29767
6	12.952	1241.66	13.979		XM64	=	0.09986
16	4.586	676.80	14.796		P63/P6	=	0.99000
64	17.539	1099.04	13.919		P163/P16	=	0.99000
8	17.539	1099.04	13.639	27.509	A8	=	80.66 in²
Bleed	0.000	676.80	16.041		CD8	=	1.00000

Efficiencies:	isentr	polytr	RNI	P/P			
					P8/Pamb	=	3.94418
Outer LPC	0.8739	0.8911	0.408	2.892	WLkBy/W25=		0.00000
Inner LPC	0.8739	0.8911	0.408	2.892	W_NGV/W25=		0.06000
HP Compressor	0.8469	0.8897	0.795	13.782	WHcl/W25 =		0.00000
Burner	0.9935			0.960	Loading	=	323.10 %
HP Turbine	0.8780	0.8490	2.546	6.855	e444 th	=	0.87819
LP Turbine	0.8900	0.8795	0.605	2.173	WLcl/W25	=	0.00000
Mixer	0.9000				WBHD/W21	=	0.00000
					far7	=	0.00850
HP Spool mech Eff 0.9900		Speed		32760 rpm	WBLD/W25	=	0.00000
LP Spool mech Eff 0.9900		Speed		18686 rpm	PWX	=	0.0 hp
					P16/P13	=	0.9587

Figure A.4.

Supersonic Dash (AB=2450R)

Station	W lb/s	T R	P psia	WRstd lb/s			
amb		416.97	2.720		FN	=	1500.87 lb
1	21.760	558.10	7.539				
02	7.259	558.10	7.539	32.358	TSFC	=	1.6591 lb/(lb*h)
12	2.611	558.10	7.254	12.098	P02/P1	=	1.00000
2	21.760	558.10	7.464	44.443	P12/P1	=	0.96220
13	5.757	777.21	20.718	4.999	WF Burner=		0.21167 lb/s
21	16.003	777.21	21.532	13.370	s NOX	=	1.8351
25	16.003	777.21	21.532	13.370	BPR	=	0.3597
3	15.043	1711.80	293.425	1.369	Core Eff =		0.5607
31	14.082	1711.80	293.425		Prop Eff =		0.5523
4	14.294	2619.53	281.677	1.676	P3/P2	=	39.313
41	15.254	2565.39	281.677	1.770	P16/P6	=	1.05899
43	15.254	1732.22	41.211		A63	=	431.60 in²
44	15.254	1732.22	41.211		A163	=	31.44 in²
45	16.214	1679.58	40.836	10.500	A64	=	463.04 in²
49	16.214	1414.66	18.941		XM63	=	0.08479
5	16.214	1414.66	18.941	20.776	XM163	=	0.29880
6	16.214	1414.66	18.754		XM64	=	0.10001
16	5.757	777.21	19.860		P63/P6	=	0.99000
64	21.971	1254.01	18.676		P163/P16	=	0.99000
7	10.184	2450.00	18.543		WF total =		0.69168 lb/s
8	22.451	2450.00	18.543	38.672	A8	=	115.68 in²
Bleed	0.000	777.21	21.532		CD8	=	1.00000

Efficiencies:	isentr	polytr	RNI	P/P			
					P8/Pamb	=	6.81714
Outer LPC	0.8842	0.8997	0.466	2.856	WLkBy/W25=		0.00000
Inner LPC	0.8842	0.8997	0.466	2.856	W_NGV/W25=		0.06000
HP Compressor	0.8500	0.8913	0.905	13.627	WHcl/W25 =		0.00000
Burner	0.9977			0.960	Loading	=	169.09 %
HP Turbine	0.8795	0.8518	2.961	6.835	e444 th	=	0.87983
LP Turbine	0.8925	0.8826	0.697	2.156	WLcl/W25	=	0.00000
Mixer	1.0000				WBHD/W21	=	0.00000
Reheat	0.8848			0.993	WF Reheat=		0.48001 lb/s
					XM64	=	0.10001
					XM7	=	0.14829

Figure A.5.

Loiter (Throttle=96.7%)

Station	W lb/s	T R	P psia	WRstd lb/s			
amb		492.18	8.294		FN	=	1234.92 lb
1	29.672	516.83	9.838		TSFC	=	0.7714 lb/(lb*h)
02	9.905	516.83	9.838	32.560	P02/P1	=	1.00000
12	3.554	516.83	9.466	12.143	P12/P1	=	0.96213
2	29.672	516.83	9.740	44.691	WF Burner=		0.26461 lb/s
13	7.836	722.86	27.140	5.009	s NOX	=	1.5089
21	21.836	722.86	28.209	13.430	BPR	=	0.3588
25	21.836	722.86	28.209	13.430	Core Eff =		0.4523
3	20.526	1604.57	387.005	1.371	Prop Eff =		0.4513
31	19.216	1604.57	387.005				
4	19.480	2452.69	371.460	1.676	P3/P2	=	39.734
41	20.790	2401.89	371.460	1.770	P16/P6	=	1.05927
43	20.790	1612.38	53.997		A63	=	431.60 in²
44	20.790	1612.38	53.997		A163	=	31.44 in²
45	22.101	1562.74	53.503	10.537	A64	=	463.04 in²
49	22.101	1310.65	24.802		XM63	=	0.08474
5	22.101	1310.65	24.802	20.816	XM163	=	0.29927
6	22.101	1310.65	24.556		XM64	=	0.09993
16	7.836	722.86	26.012		P63/P6	=	0.99000
64	29.936	1162.33	24.454		P163/P16 =		0.99000
8	29.936	1162.33	23.964	27.483	A8	=	80.66 in²
Bleed	0.000	722.86	28.209		CD8	=	1.00000

Efficiencies:	isentr	polytr	RNI	P/P			
					P8/Pamb	=	2.88943
Outer LPC	0.8779	0.8944	0.666	2.867	WLkBy/W25=		0.00000
Inner LPC	0.8779	0.8944	0.666	2.867	W_NGV/W25=		0.06000
HP Compressor	0.8512	0.8924	1.293	13.719	WHcl/W25 =		0.00000
Burner	0.9976			0.960	Loading =		170.98 %
HP Turbine	0.8792	0.8507	4.209	6.879	e444 th	=	0.87942
LP Turbine	0.8997	0.8902	0.992	2.157	WLcl/W25 =		0.00000
Mixer	0.9000				WBHD/W21 =		0.00000
					far7	=	0.00892
HP Spool mech Eff 0.9900		Speed		33845 rpm	WBLD/W25 =		0.00000
LP Spool mech Eff 0.9900		Speed		19225 rpm	PWX	=	0.0 hp
					P16/P13 =		0.9584

Figure A.6.

Appendix B – Fan and Compressor; Additional Information

Inlet	Radius	Mach Axial	Mach Relative	Turning Angle (°)
Rotor 1	8.80	0.50	1.38	37.10
Stator 1	7.53	0.61	1.21	24.70
Rotor 2	7.40	0.60	1.16	34.41
Stator 2	6.65	0.60	1.05	33.80
Rotor 3	6.50	0.61	1.02	22.41
Stator 3	6.05	0.56	0.93	41.52
Fan Exit	6.00	0.51		

Table A.1. Flow Parameters at Fan Tip

Inlet	Radius	Mach Axial	Mach Relative	Turning Angle (°)
Rotor 1	4.35	0.5	0.81	58.69
Stator 1	4.32	0.61	0.85	56.00
Rotor 2	4.19	0.6	0.82	57.17
Stator 2	4.06	0.6	0.80	50.00
Rotor 3	3.94	0.606	0.78	43.04
Stator 3	3.89	0.56	0.74	41.59
Fan Exit	3.72	0.51		

Table A.2. Flow Parameters at Fan Hub

Inlet	Radius	Mach axial	Mach relative	Turning Angle (°)
Rotor 1	5.25	0.51	1.39	54.80
Stator 1	4.80	0.76	1.24	22.00
Rotor 2	4.80	0.80	1.28	38.57
Stator 2	4.60	0.66	1.15	23.00
Rotor 3	4.55	0.69	1.11	34.31
Stator 3	4.40	0.56	1.09	30.00
Rotor 4	4.30	0.61	0.98	24.35
Stator 4	4.15	0.53	1.06	34.00
Rotor 5	4.05	0.53	0.87	18.69
Stator 5	3.85	0.49	1.03	30.00
Rotor 6	3.75	0.43	0.77	6.77
Stator 6	3.60	0.37	1.13	32.14
Compressor Exit	3.50	0.30		

Table A.3. Flow Parameters at Compressor Tip

Inlet	Radius	Mach	Mach relative	Turning Angle (°)
Rotor 1	3.24	0.51	0.95	76.43
Stator 1	3.64	0.76	0.86	39.50
Rotor 2	3.71	0.8	1.11	47.11
Stator 2	3.76	0.66	0.81	31.50
Rotor 3	3.74	0.69	0.99	40.06
Stator 3	3.75	0.56	0.79	35.70
Rotor 4	3.69	0.61	0.90	27.81
Stator 4	3.67	0.53	0.77	45.00
Rotor 5	3.57	0.53	0.81	18.51
Stator 5	3.47	0.49	0.75	45.00
Rotor 6	3.33	0.43	0.72	5.90
Stator 6	3.25	0.37	1.01	14.86
Compressor Exit	3.08	0.3		

Table A.4. Flow Parameters at Compressor Hub

	Inlet Angle	Exit angle (°)
Rotor 1	59.8	22.7
Stator 1	52.2	27.5
Rotor 2	48.6	14.2
Stator 2	49.7	15.9
Rotor 3	46.6	24.2
Stator 3	41.5	0

Table A.5. Blade Metal Angles at Fan tip

	Inlet Angle	Exit angle (°)
Rotor 1	58.3	15.0
Stator 1	47.1	11.1
Rotor 2	47.7	5.6
Stator 2	46.5	8.5
Rotor 3	42.9	12.0
Stator 3	41.4	0

Table A.6. Blade Metal Angles at Fan Pitch

	Inlet Angle	Exit angle (°)
Rotor 1	57.0	-4.6
Stator 1	46.7	-9.2
Rotor 2	47.7	-9.3
Stator 2	46.1	-3.8
Rotor 3	41.4	-1.6
Stator 3	41.5	0

Table A.7. Blade Metal Angles at Fan Hub

Inlet	Inlet Angle	Exit Angle
Rotor 1	66.2	11.4
Stator 1	49.15528	27.1
Rotor 2	36.4	-2.1
Stator 2	54.5	31.5
Rotor 3	32.6	-1.6
Stator 3	55.9	25.9
Rotor 4	37.7	13.4
Stator 4	48.9	14.9
Rotor 5	46.2	27.5
Stator 5	39.5	9.5
Rotor 6	52.0	45.2
Stator 6	32.1	0

Table A.8. Blade Metal Angles at Compressor Tip

Inlet	Inlet Angle	Exit Angle
Rotor 1	64.9	0.5
Stator 1	49.8	19.8
Rotor 2	36.8	-5.4
Stator 2	53.1	26.1
Rotor 3	33.0	-3.6
Stator 3	54.5	21.5
Rotor 4	37.7	12.1
Stator 4	47.4	7.4
Rotor 5	47.7	29.6
Stator 5	35.4	3.4
Rotor 6	52.6	44.8
Stator 6	29.4	0

Table A.9. Blade Metal Angles at Compressor Pitch

Inlet	Inlet Angle	Exit Angle
Rotor 1	66.1	-10.2
Stator 1	50.4	10.9
Rotor 2	37.6	-9.4
Stator 2	52.0	20.5
Rotor 3	33.3	-6.7
Stator 3	53.5	17.8
Rotor 4	37.2	9.4
Stator 4	46.6	1.6
Rotor 5	48.4	29.8
Stator 5	32.6	-12.3
Rotor 6	56.4	50.5
Stator 6	14.8	0

Table A.10. Blade Metal Angles at Fan Compressor Hub

Acknowledgments

References

[1]Jenkinson, L.R., "Aircraft Design Projects for Engineering Students," Oxford: Butter-Worth Heinemann, 2003

[2]Mattingly, J.D. Hever, W.H., and Pratt, D.T., "Aircraft Engine Design," *J.S. Przemieniecki Ed.*, AIAA, Reston Virginia, 2002.

[3]*"GasTurb 12: A Design & Off-Design Performance Program for Gas Turbines"*, http://www.gasturb.de, Joachim Kurzke, 2012.

[4]Jane's Information Group, "Further Development and Applications of Stiffness Method," *Jane's Aero-Engines*, Alexandria, VA, 1963, pp. 6–10.

[5]Wilson, David Gordon, and Korakianitis, Theodosios, "The Design of High-Efficiency Turbomachinery and Gas Turbines," *Second Edition*, Upper Saddle River, NJ, 1998.

[6]Koch, C. C., "Stalling Pressure Rise Capability of Axial Flow Compressor Stages," *Journal of Engineering for Power Vol. 103*, ASME, October, 1981.

[7]Calvert, W.J., and Ginder, R.B., "Transonic Fan and Compressor Design," *Proceedings of the Institution of Mechanical Engineers Vol. 213 Part C*, C02098, 1999.

[8]Koch, C.C., and Smith, Jr., L.H., "Loss Sources and Magnitudes in Axial-Flow Compressors," *Journal of Engineering for Power*, ASME, July, 1976.

[9]Wisler, D.C., Koch, C.C., and Smith, Jr., L.H., "Preliminary Design Study of Advanced Multistage Axial Flow Core Compressors," NASA CR 135133 R77AEG222, Submitted by General Electric, February, 1977.

[10]Holloway, P.R., Knight, G.L., Koch, C.C., and Shaffer, S.J., "Energy Efficient Engine High Pressure Compressor Detail Design Report," NASA CR-165558, Submitted by General Electric, 1988.

[11]Lefebvre, Arthur H. and Ballal, Dilip R., "Gas Turbine Combustion," *Alternative Fuels and Emissions*, Taylor and Francis Group, Boca Raton, FL, 2010.

[12]Stickles, Rick, and Barrett, Jack, "TAPS II Combustor Final Report – Continuous Lower Energy, Emissions, and Noise (CLEEN) Program," Federal Aviation Administration DTFAWA-10-C-00046, Submitted by General Electric, 2013.
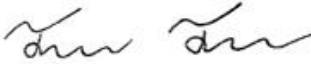
[13]Mckinney, Randal G., Sowa, William, and Cheung, Albert K., "The Pratt & Whitney TALON X Low Emissions Combustor: Revolutionary Results with Evolutionary Technology," *45th AIAA Aerospace Sciences Meeting and Exhibit*, AIAA 2007-386, Reno, Nevada, 2007.

[14]Fouse, Michael J., Thomas, Doug, Stickles, Rick, Cooper, Clay, and Dodds, Will, "Development of the GE Aviation Low Emissions TAPA Combustor for Next Generation Aircraft Engines," *50th AIAA Aerospace Sciences Meeting including the New Horizons Forum and Aerospace Exposition*, AIAA 2012-0936, Nashville, Tennessee, 2012.

[15]Mohammed, B.S., and Jeng, S.M., "Design Procedures and a Developed Computer Code for Preliminary Single Annular Combustor Design," *45th AIAA/ASME/SAE/ASEE Joint Propulsion Conference and Exhibit*, AIAA 2009-5208, Denver, Colorado, 2009.

[16]Younossi, Obaid, Arena, Mark, "Technology Basics and Cost-Estimating Methodology," *Military Jet Engine Acquisition,* F49642-01-C-0003, Santa Monica, CA, 2002.

Signature Page

Name	AIAA Number	Signature
Michael Denton	448347	
Richard Zelinski	688287	
Seth Young	688197	
Trace Taylor	448300	
Vaughn Bostwick	688241	